國 立 交 通 大 學

電機與控制工程學系

碩士論文

以史都華平台為基礎之駕駛模擬器

A Driving Simulator Based on Stewart Platform

研究生：吳東璋

指導教授：李祖添 博士

中華民國 93 年 6 月

以史都華平台為基礎之駕駛模擬器

研究生：吳東璋　　指導教授：李祖添 博士

國立交通大學電機與控制工程學系

摘要

史都華平台為一個具有六自由度運動之機械平台。由於其並列式結構的特點，相較於傳統串列式結構操作器，史都華平台具有更高的力重比、剛性和控制精度。本論文主要的目的為在史都華平台有限的工作空間下，達到模擬逼近真實的效果。其中包括汽車動態模型的建立，沖淡濾波器和逆向動力學。首先確定所要模擬的駕駛情況，透過沖淡濾波器所得到平台的運動軌跡，同時將規劃的平台運動軌跡透過逆向動力學算出六隻致動器在運動過程中所承受的負載，並檢驗運動過程中是否超出油壓系統所能提供的最大動力，最後設計一個 PID 控制器讓致動器在高負載的情況下運動能有好的成果。模擬結果顯示出所提出方法之可行性。

A driving simulator based on Stewart platform

Student：Tung-Chang Wu　　Advisor：Tsu-Tian Lee

Department of Electrical and Control Engineering
National Chiao Tung University

Abstract

Stewart platform is a mechanism with six degree of freedom. Because of its feature of parallel structure, Stewart platform offers higher force-to-weight ratio, higher stiffness and control accuracy over conventional serial manipulator. This thesis presents a study of a driving simulator based on Stewart platform. The main purpose is to make simulation more realistic without driving out of its limited workspace. This thesis presents a car dynamic model, washout filter, and inverse dynamics of Stewart platform. First, goal is to make sure of the driving situation and obtain the corresponding motion trajectory of Stewart platform through washout filter; secondly to figure out six actuators' external load force by inverse dynamics and make sure that it's under the maximum power which hydraulic system can offer. Finally, a PID controller will be designed to obtain good performance when actuator moves under high load. Simulation results show the applicability of the proposed method.

誌　　謝

承蒙　指導教授李祖添教授二年來的悉心指導與生活上的照顧，使得愚生不論在學業或待人處事上都受益良多，生活上也得以紓減經濟壓力，在此致上最深的謝意與敬意。此外要感謝杜國洋教授的指導，讓我在研究過程中所遇到的問題能夠迎刃而解，得以順利完成本論文。也謝謝 805 實驗室的所有成員，因為有你們在生活、學業上的教學相長，陪我度過了值得紀念的碩士班生活。

最後要謝謝我的父母及家人二年來的支持與鼓勵，做為我最大的後盾，使我能克服所有的難關，順利完成學業，僅以此書獻給所有關心我家人、朋友與同學。

Contents

List of Tables

List of Figures

Chapter 1

Introduction

1.1 Motivation

Motion simulators integrated with the technology of virtual reality and motion platform are widely used in military simulation, entertainment, education training, etc. It is convenient and safe that training courses won't be limited by the factor of weather or location. And simulation situation can be changed if needed. For training pilot to operate some expensive or huge transportation, motion simulators have the function of decreasing training cost and shortening training time.

The main purpose of this thesis is to design a driving simulator base on Stewart platform. Simulation can be felt realistic if motion platform can move what a vehicle does. In this way, Pilot can feel the same motion sensation of linear or rotation by moving platform as driving a car when pilot operates simulator. However, workspace of Stewart platform is limited. In order to give pilot motion sensation as realistic as possible and simplify the motion trajectory without driving out of workspace of Stewart platform, washout filter is the key point. Besides, the summation of six actuators' force can't exceed the maximum power which hydraulic system can offer during motion process. The force can be viewed as external disturbance force of six actuators. We need to design a controller that Stewart platform offers good performance under this high disturbance force.

1.2 Literature review

The Stewart platform is a six-degree-of-freedom mechanism with upper and lower platforms connected together by six extensible actuators. Originally, it is proposed by Stewart [1] in 1965 as a flight simulator. Because of the parallel structure of the Stewart platform, it has the advantages of higher strength-to-weight ratios, stiffness, high precision positioning capability, and simple inverse kinematics as compared to conventional open-chain serial manipulators. Contrarily, it has small workspace, low maneuverability, and complex forward kinematics. In last decades, the research about the Stewart platform can be listed as follows：

(1) In 1984, Yang and Lee [2] presented the inverse kinematics of the Stewart platform.

(2) In 1986, Fichter [3] derived the kinematic equations of the Stewart platform and stated the condition of singularity along with the enumeration of a few singular configurations.
(3) In 1988, Do and Yang [4] solved the inverse dynamics for the Stewart platform by the Newton-Euler approach assuming the joints as frictionless and legs as symmetrical and thin.
(4) In 1991, Liu [5] developed Lagrangian equations of motion under some simplifying assumptions regarding the geometry and inertia distribution of the manipulator.
(5) In 1991, Nguyen, Zhou, and Antrazi [6] used Newton-Raphson method to solve the forward kinematics of the Stewart platform addressing the problem of efficient computation. They also developed the transformation, Jacobian matrix, which transforms the actuator lengths into the Cartesian position and orientation of the payload platform with respect to the base platform.
(6) In 1993, Liu, Fitzgerald, and Lewis [7] proposed a simplified algorithm which involves only three nonlinear simultaneous equations to solve the forward kinematics of Stewart platform.
(7) In 1993, Ji [8] considered the effect of leg inertia of the dynamics of the Stewart platform.
(8) In 1998, Dasgupta and Mruthyunjaya [9] developed an efficient inverse dynamics formation, gravity and viscous friction forces at the joints for the Stewart platform.

Besides the Stewart platform, motion cueing algorithm, the so-called washout filter, also plays an important role in driving simulator. In 1997, Grant and Reid [10] discussed the tuning rules and requirements of the coefficients of the washout filter. Nahon and Reid [11] presented a comparison of three different kinds of washout filter from the designer's viewpoint.

1.3 Brief sketch of the contents

The reminder of the thesis is organized as follows. First, kinematics and dynamics of Stewart platform are included in chapter 2. Chapter 3 describes the principle of washout filter and two half-car dynamic model. Chapter 4 provides eletro-hydraulic system, the simulation blocks of a driving simulator, and the simulation results. Finally, conclusions are given in chapter 5.

Chapter 2

Kinematics and dynamics of Stewart platform

Fig. 2-1 The Stewart Platform

2.1 Preface

Fig. 2-1 and 2-2 show the Stewart Platform which mainly consists of a base platform, a payload platform, and six linear actuators. In this chapter, we will give a detailed description of the inverse kinematics [2], the forward kinematics [6], and the inverse dynamics of Stewart Platform [9] as follows. The inverse kinematics determines the required actuator lengths for a given configuration of Cartesian position and orientation of payload platform with respect to the base platform. The forward kinematics transforms the actuator length into the Cartesian position and orientation of the payload platform with respect to the base platform. Finally, the inverse dynamics of the Stewart Platform has been formulated.

2.2 Inverse Kinematics [2]

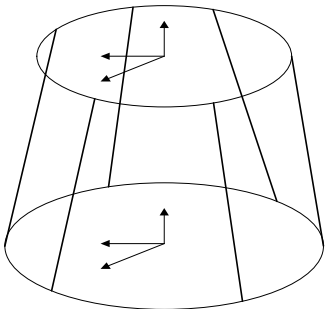

Fig. 2-2 The Stewart Platform frame assignments

This section deals with the inverse kinematics of the Stewart Platform. As shown in Fig. 2-2, frame assignment to the platform is demonstrated that two coordinate frames {P}, and {B} are assigned to the payload and base platforms, respectively. The origin of frame {B} is located at the center of the payload platform. And the origin of frame {B} is located at the center of the base platform. The Cartesian variables are chosen to be the relative position and orientation of frame {P} with respect to frame {B}. And the position of frame {P} is specified by the position of its origin with respect to frame {B}. Then, we can define vector ${}^{p}p_i = [p_{ix} \quad p_{iy} \quad p_{iz}]^T$ as the position of the attachment point p_i with respect to frame {P}, and vector ${}^{B}B_i = [b_{ix} \quad b_{iy} \quad b_{iz}]^T$ as the position of the attachment point B_i with respect to frame {B} for i = 1, 2,…,6. We continue to consider the vector diagram as shown in Fig. 2-3. The platform connection point p_4 can be transformed to base frame by use the platform translation, t, and rotation matrix, $\Re$, relative to the base as

$$ {}^{B}p_4 = \Re\, {}^{p}p_4 + t \tag{2.1} $$

Then, the leg vector, S_4, can be found from the difference of the position vectors of the platform point and the base point. Thus, we obtain

$$ S_4 = \Re\, {}^{p}p_4 + t - B_4 = \Re \cdot \begin{bmatrix} p_{4x} \\ p_{4y} \\ p_{4z} \end{bmatrix} + \begin{bmatrix} x \\ y \\ z \end{bmatrix} - \begin{bmatrix} b_{4x} \\ b_{4y} \\ b_{4z} \end{bmatrix} = \begin{bmatrix} u_4 \\ v_4 \\ w_4 \end{bmatrix} + \begin{bmatrix} x \\ y \\ z \end{bmatrix} - \begin{bmatrix} b_{4x} \\ b_{4y} \\ b_{4z} \end{bmatrix} = \begin{bmatrix} u_4 + x - b_{4x} \\ v_4 + y - b_{4y} \\ w_4 + z - b_{4z} \end{bmatrix} \tag{2.2} $$

$$ L_4 = \|S_4\| = \sqrt{(u_4 + x - b_{4x})^2 + (v_4 + y - b_{4y})^2 + (w_4 + z - b_{4z})^2} \tag{2.3} $$

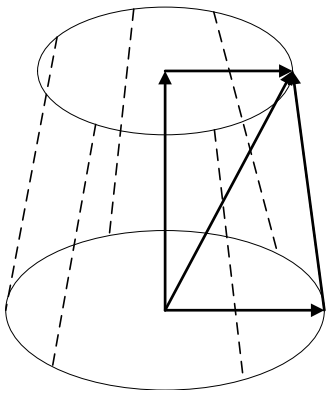

Fig. 2-3 Vector diagram

Equation (2.3) represents the closed-form solution to the inverse kinematics problem. And the actuator length l_i can be determined by equation (2.3) for i = 1, 2,… ,6. The orientation of frame {P} with respect to frame {B} described by the orientation matrix, $\Re$, in (2.1) is given by

$$\Re = \begin{bmatrix} \cos\beta\cdot\cos\gamma + \sin\alpha\cdot\sin\beta\cdot\sin\gamma & -\cos\beta\cdot\sin\gamma + \sin\alpha\cdot\sin\beta\cdot\cos\gamma & \cos\alpha\cdot\sin\beta \\ \cos\alpha\cdot\sin\gamma & \cos\alpha\cdot\cos\gamma & -\sin\alpha \\ -\sin\beta\cdot\cos\gamma + \sin\alpha\cdot\cos\beta\cdot\sin\gamma & \sin\beta\cdot\sin\gamma + \sin\alpha\cdot\cos\beta\cdot\cos\gamma & \cos\alpha\cdot\cos\beta \end{bmatrix} \tag{2.4}$$

Angle, α, β, and γ represent the orientation of frame {P} with respect to frame {B} about X_B, Y_B, and Z_B axes respectively. Finally, we apply the inverse kinematics to find out the workspace of the Stewart Platform. Because of the difference between the mechanical structures of each Stewart Platform, the workspace is different. The Stewart Platform we bought is not a sphere. The upper-half workspace and vertical view are shown in Fig. 2-4 and Fig 2-5, respectively.

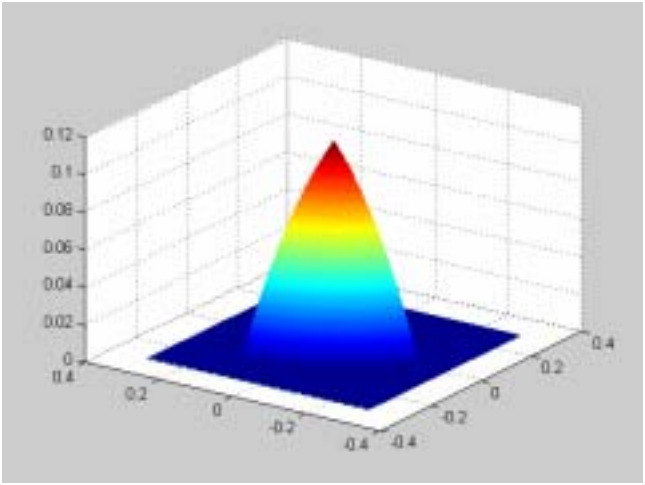

Fig. 2-4 The upper-half workspace of Stewart Platform

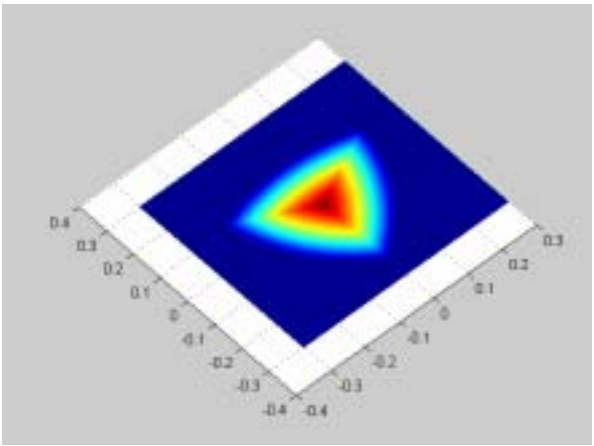

Fig. 2-5 The vertical view of the Stewart Platform

2.3 Forward Kinematics [6]

This section deals with the forward kinematics which transforms the actuator lengths l_i for i = 1, 2, … 6 into the Cartesian position and orientation of the payload platform with respect to the base platform. The forward kinematics can be considered as to find a Cartesian position specified by x, y, z and an orientation specified by angle α、β、and γ to satisfy equation (2.3) for a set of actuator lengths l_i for i = 1, 2, … 6. Usually, there is no closed-form solution for the problem since there are six nonlinear equations with six unknowns. But we know the initial Cartesian position and orientation before the platform is working, Newton-Raphson method is practicable. In the following, we will present the Newton-Raphson method for solving the forward kinematics.

From equation (2.3) we can define 6 functions

$$f_i(a) = (u + x - b_{ix})^2 + (v + y - b_{iy})^2 + (w + z - b_{iz})^2 - L_i{}^2 = 0 \qquad (2.5)$$

for i = 1, 2, … 6. And the vector a is defined as

$$a = [x \quad y \quad z \quad \alpha \quad \beta \quad \gamma]^T \qquad (2.6)$$

that is the Cartesian position and orientation we want to solve. Then, follows the following steps to solve for the equation (2.5)

Step 1. Get the initial Cartesian position and orientation

Step 2. Compute the rotation matrix $\Re$ and u_i、v_i、w_i in equation (2.2) for i = 1, 2, … 6

Step 3. Compute $F = f_i(a)$ and $Z_{ij} = \dfrac{\partial f_i}{\partial a_j}$ using equation (2.5) for i, j = 1, 2,…, 6.

Step 4. Compute $Z^{-1} * F$. If the maximum element of $Z^{-1} * F$ < tolerance, then stop the iteration and $a^{new} = a - Z^{-1} * F$

Step 5. $a^{new} = a - Z^{-1} * F$ and repeat Steps 1-5

2.4 Inverse dynamics [9]

This section considers the dynamics of the legs and identifies the contribution of each leg acting on the platform. Then, the dynamics of the platform and solution of the required leg forces will be determined. The following notations have been used in this section.

$t = translation\ vector$ ($position\ of\ \ platform$)

$\Re = rotation\ matrix$ ($orientation\ of\ \ platform$)

$\dot{t} = linear\ velocity\ of\ \ reference\ \ point\ of\ \ platform$

ω = angular velocity of platform

$\ddot{t}$ = linear acceleration of reference point of platform

α = angular acceleration of platform

W = angular velocity of the leg

M = mass of platform

R_0 = center of gravity of platform (in platform frame)

I_p = moment of inertia of platform (in platform frame)

F_{ext} = external force on the platform (in platform frame)

M_{ext} = external moment on the platform (in platform frame)

B_i = ith base point

k_i = stationary axis of the universal joint at ith leg

p_i = ith platform point (in platform frame)

$q_i = \Re p_i$

T_i = rotation matrix giving orientation of ith leg

$(m_d)_i, (m_u)_i$ = masses of lower and upper part of ith leg

$(r_{d0})_i, (r_{u0})_i$ = CG of lower and upper part of ith leg (in local frames)

$(I_{d0})_i, (I_{u0})_i$ = moments of inertia of lower and upper part of ith leg (in local frame)

g = acceleration due to gravity

C_u, C_p, C_s = coefficients of viscous friction in the universal, prismatic and spherical joints, respectively

F_i = input force required at ith leg

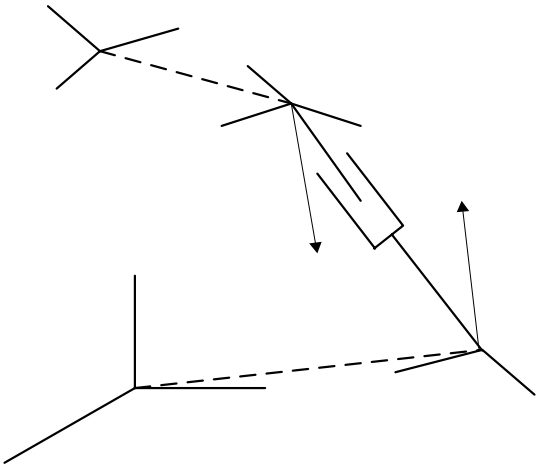

Fig. 2-6 Details of one leg

One leg of the Stewart Platform has been shown in Fgi.2-4 with the associated symbols. Besides two frames, frame {B} and frame {p} mentioned before, two other frames of reference, namely frame D and frame U, have been shown which are attached to the lower and upper parts of the legs. Furthermore, the leg index, i, has been dropped from the equation for convenience in this section. From equation (2.2), we have known that the platform connection point can be transformed to base frame as

$$S = \Re p + t - B \tag{2.7}$$

The leg length and the unit vector along the leg are given by

$$L = \|S\| \tag{2.8}$$

$$s = S / L \tag{2.9}$$

The velocity of the platform connection point is the time derivative of the leg vector and is given in terms of the platform velocities as

$$\dot{S} = \omega \times q + \dot{t} \tag{2.10}$$

The sliding velocity between the two parts of the leg can be formulated as

$$\dot{L} = s \cdot \dot{S} \tag{2.11}$$

The angular velocity W related to the component of $\dot{S}$ perpendicular to the leg is given as

$$W \times S = \dot{S} - \dot{L}s \tag{2.12}$$

Take the cross product of the equation (2.12), we obtain

$$W = s \times \dot{S} / L \tag{2.13}$$

The time derivative of $\dot{S}$ is the acceleration of the platform connection point and is expressed as

$$\ddot{S} = \alpha \times q + \omega \times (\omega \times q) + \ddot{t} \tag{2.14}$$

Similarly, The time derivative of $\dot{L}$ is the sliding acceleration between the upper and the lower parts of the leg.

$$\ddot{L} = s \cdot \ddot{S} + LW \cdot W \tag{2.15}$$

A frame of reference (frame D shown in Fig. 2-4) is attached to the lower part of the leg with its origin at the base point, x-axis along the leg, y-axis along the rotating axis (axis fixed to the leg) and z-axis perpendicular to the x and y axes according to the right hand rule. Another frame of reference (frame U shown in Fig. 2-4) is attached to the upper part of the leg with the origin at the platform by the same orientation rule. The dynamics of the leg have to be transformed to a fixed frame of reference. And the fixed frame of reference has to be parallel to the base frame at the base point.

It is just a rotation to transform the moving lower frame to the fixed leg frame. The x, y, and z axes of the moving lower frame are

$$x-axis: \quad \hat{x} = s$$

$$y-axis: \quad \hat{y} = (k \times s)/\|k \times s\|$$

$$z-axis: \quad \hat{z} = \hat{x} \times \hat{y}.$$

And the transformation matrix is

$$T = [\hat{x}\ \hat{y}\ \hat{z}]. \tag{2.16}$$

It is the same rotation matrix to transformation from the moving upper frame to fixed leg frame. Then, r_{d0} and r_{u0} present the position vectors of the center of gravity of the lower and the upper parts in D and U frames. They can also be transformed to the fixed leg frame as

$$r_d = Tr_{d0} \tag{2.17}$$

$$r_u = T(v + r_{u0}) \tag{2.18}$$

where

$$v = [L\ 0\ 0]^T. \tag{2.19}$$

The acceleration of the center of gravity of the two parts are

$$a_d = A \times r_d + W \times (W \times r_d) \tag{2.20}$$

$$a_u = \ddot{L}s + A \times r_u + W \times (W \times r_u) + 2\dot{L}W \times s \tag{2.21}$$

where

$$A = (s \times \ddot{S} - 2\dot{L}W)/L. \tag{2.22}$$

The moment of inertia, I_d, of the lower part in its fixed leg frame can be obtained from its moment of inertia, I_{d0}, in its local frame by the rotation transformation

$$I_d = TI_{d0}T^T. \tag{2.23}$$

The transformation of the moment of inertia of the upper part involves a rotation as well as a translation

$$I_u = T[I_{u0} + m_u L^2 diag(0,1,1)]T^T. \tag{2.24}$$

The moment of viscous friction at the joint is given as

$$f = C_s\ (W - \omega). \tag{2.25}$$

Consider the moments acting on the lower part of the leg in the fixed frame, by Euler's equation, it is given as

$$-m_d r_d \times a_d + m_d r_d \times g - I_d A - W \times I_d W + M_u s - r \times F_p - M_p - C_u W = 0 \tag{2.26}$$

where M_u is the magnitude of the constraint moment at the upper joint, F_p is the

vector force at the prismatic joint exerted by the lower part on the upper part acting at a point r, M_p is the vector moment at the prismatic joint acting on the upper part and the moment of viscous friction at the upper joint is the last term in the equation. Similarly, the upper part of the leg is given by Euler's equation as

$$-m_u r_u \times a_u + m_u r_u \times g - I_u A - W \times I_u W + S \times F_s + r \times F_p + M_p - f = 0 \qquad (2.27)$$

We can obtain Euler's equation for the whole leg by combining equation (2.26) and (2.27) as

$$\begin{aligned} &- m_d r_d \times a_d - m_u r_u \times a_u + (m_d r_d + m_u r_u) \times g - (I_d + I_u) A \\ &- W \times (I_d + I_u) W + M_u s + S \times F_s - C_u W - f = 0 \end{aligned} \qquad (2.28)$$

or

$$M_u + S \times F_s = C \qquad (2.29)$$

where

$$C = m_d r_d \times a_d + m_u r_u \times a_u - (m_d r_d + m_u r_u) \times g + (I_d + I_u) A + W \times (I_d + I_u) W + C_u W + f \qquad (2.30)$$

In order to eliminate the unknown scalar M_u from equation (2.29), we can take cross products with s, then we can obtain

$$s \times (S \times F_s) = s \times C \qquad (2.31)$$

or

$$F_s = xs + \frac{C \times s}{L} = xs + K \qquad (2.32)$$

where $x = s \cdot F_s$ is the component of the force F_s at the lower joint along the leg and

$$K = \frac{C \times s}{L} \qquad (2.33)$$

Finally, we take the upper part of the leg into consideration and it is given by Newton's equation as

$$-m_u a_u + m_u g + F_p + F_s - C_p \dot{L} s = 0 \qquad (2.34)$$

where $C_p \dot{L} s$ is the viscous resistance at the prismatic joint.

We can take the dot product of the above equation with s. Then, we can obtain the component of the above equation in the direction of the leg as

$$s \cdot F_p = m_u s \cdot (a_u - g) + C_p \dot{L} - s \cdot F_s \qquad (2.35)$$

We can obtain the actuator force, F, by substituting from equation (2.33) above

$$F = D - x \tag{2.36}$$

where

$$D = m_u s \cdot (a_u - g) + C_p \dot{L} . \tag{2.37}$$

In the proceeding, the complete dynamic equations for a leg have been given. Then, the dynamic equations for the Stewart Platform will be developed as six linear equations. First, we take the acceleration and inertia of the platform into consideration. Let R_0 be the position vector of the center of gravity of the Stewart Platform with respect to the local frame, then the same vector with respect to the base frame can be expressed as

$$R = \Re R_0 . \tag{2.38}$$

The acceleration of the center of gravity is

$$a = \alpha \times R + \omega \times (\omega \times R) + \ddot{t} . \tag{2.39}$$

The moment of inertia, I_p, of the Stewart Platform can be transformed to the global basis as

$$I = \Re I_p \Re^T . \tag{2.40}$$

From Newton's equation, the equation for the Stewart Platform can be written as

$$-Ma + Mg + \Re F_{ext} - \sum_{i=1}^{6} (F_s)_i = 0 . \tag{2.41}$$

We can express the equation in different way by substituting $(F_s)_i$ from equation (2.32)

$$\sum_{i=1}^{6} x_i s_i = \Re F_{ext} + M(g - a) + \sum_{i=1}^{6} K_i . \tag{2.42}$$

Taking the moments about the platform reference point and Substituting from equation (2.32) again, Euler's equation for the Stewart Platform gives

$$\sum_{i=1}^{6} [x_i q_i \times s_i] = MR \times (g - a) - I\alpha - \omega \times I\omega + \Re M_{ext} - \sum_{i=1}^{6} [q_i K_i - f_i] . \tag{2.43}$$

Combining equation (2.42) and (2.43), we get

$$\begin{bmatrix} s1 & s2 & s3 & s4 & s5 & s6 \\ q1\times s1 & q2\times s2 & q3\times s3 & q4\times s4 & q5\times s5 & q6\times s6 \end{bmatrix} \begin{bmatrix} x1 \\ x2 \\ x3 \\ x4 \\ x5 \\ x6 \end{bmatrix}$$

$$= \begin{bmatrix} \Re F_{ext} + M(g-a) - \sum_{i=1}^{6} K_i \\ MR\times(g-a) - I\alpha - \omega\times I\omega + \Re M_{ext} - \sum_{i=1}^{6}[q_i K_i - f_i] \end{bmatrix} \tag{2.44}$$

or

$$Hx = c\,. \tag{2.45}$$

The require input forces can be determined from equation (2.45) solved for x, and equation (2.37) solve for D as

$$F = D - x$$

where

$F = [F_1\ F_2\ F_3\ F_4\ F_5\ F_6]^T$ and $D = [D_1\ D_2\ D_3\ D_4\ D_5\ D_6]^T$.

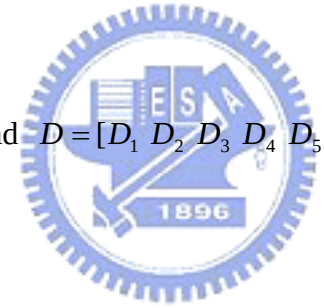

Chapter 3

Washout filter and car dynamic model

3.1 Preamble

The goal of motion simulator is to give the driver the same feeling of linear acceleration or angle velocity as when the driver operates a real vehicle. Theoretically, the driver can feel that he drives a real vehicle if a motion simulator can move exactly as a real car moves. But the problem is that a motion simulator has limited motion space. For this reason, we need the so-called washout filter to keep the motion simulator within its working space and give the driver realistic motion cues at the same time. Let the driver feel that he drives a real one.

In this chapter we will discuss the theory and framework of washout filter in detail. Then, we will introduce a car dynamic model for simulating several driving situations which will be discussed in the next chapter.

3.2 Specific force[12]

The so-called specific force is non-gravitational force per unit mass. According to Newton theory, the acceleration of the subject is the force which the subject is taken. The force includes gravitational force per unit mass and non-gravitational force per unit mass. So, specific force is the difference between inertial acceleration and gravitational acceleration. It can be formulated as

$$\vec{f} = \vec{a} - \vec{g} \tag{3.1}$$

Compared to inertial reference frame, car reference frame is a non-inertial reference frame. We can use the car model which will be introduced in this chapter to obtain the acceleration of the driver under any condition we want. The acceleration minus gravitational acceleration gives specific force which driver is taken.

3.3 The human inertial-sensing system [13] [14]

The vestibular apparatus provides people with the sensing information of motion. The main function of the vestibular apparatus is to retrieve and forward to the brain the information about the motion of the body. The vestibular apparatus possesses three semicircular canals which are responsible for the motion of angular velocity and otolith which is responsible for specific force.

As shown in Fig. 3-1 and Fig. 3-2 otolith model and semicircular canals are like a band-reject filter and a nonlinear attenuator. The threshold value of linear acceleration is about 0.17 m/s^2~0.28m/s^2. The threshold value of angle velocity is about 2.6^0/s~3.6^0/s. Without the part of nonlinear attenuation, otolith model can be written as a transfer function as

$$\frac{f'(s)}{f(s)} = \frac{K(\tau_a s+1)}{(\tau_L s+1)(\tau_S s+1)}. \tag{3.2}$$

Similarly, semicircular canals model can be written as a transfer function as

$$\frac{w'(s)}{w(s)} = \frac{T_L T_a s^2}{(T_L s+1)(T_S s+1)(T_a s+1)} \tag{3.3}$$

where the parameters such as τ_L, τ_S, τ_a and K are given in Table 3-1 and Table 3-2.

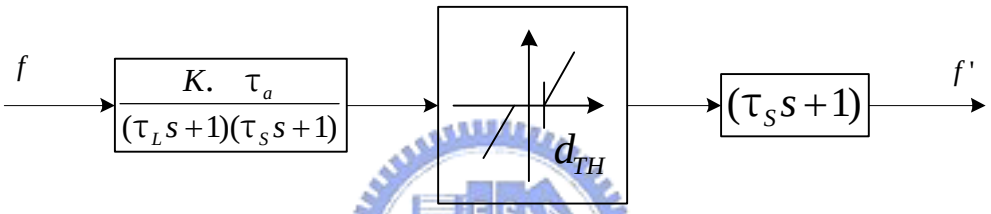

Fig. 3-1 otolith model

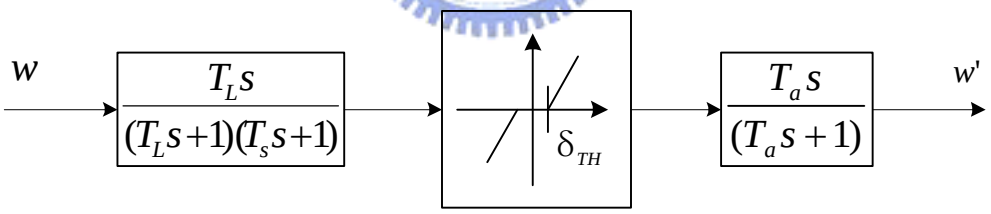

Fig. 3-2 Semicircular canals model

Table 3-1 Otolith Parameters

Parameter	A_x	A_Y	A_z	Unit
τ_L	5.33	5.33	5.33	Sec
τ_S	0.66	0.66	0.66	Sec
τ_a	13.2	13.2	13.2	Sec
K	0.4	0.4	0.4	
d_{TH}	0.17	0.17	0.28	m/sec^2

Table 3-2 Semicircular Canals Parameters

Parameter	ω_x	ω_Y	ω_z	Unit
T_L (sec)	5.3	6.1	10.2	Sec
T_S (sec)	0.1	0.1	0.1	Sec
T_a (sec)	30.0	30.0	30.0	Sec
δ_{TH}	3.6	3.0	2.6	deg/sec

3.4 Classical washout filter [10] [11]

The classical washout filter is the most widely used because of its characteristic of fixed coefficient. It is composed of two linear high-pass and one low-pass filters and break frequencies and damping ratios of three filters are adjusted by trial and error. The block diagram of the classical washout filter is shown in Fig. 3-3. The inputs of the filter are specific force, f_{AA}, and angle velocity, ω_{AA}. The outputs are the Cartesian position and orientation of the payload platform with respect to the base platform. The architecture of the classical washout filter can be divided into three parts including high-pass specific force channel, high-pass angular rate channel, and low-pass specific force channel. Three channels will be discussed later. The following notations have been used in this section.

L_{IS} = *rotation matrix that transforms vector components from the simulator reference frame to the inertial frame*

T_s = *transformation matrix from angular velocity to Euler angle rates*

f_{AA} = *body axis components of the vehicle specific force at the driver's seat reference point*

ω_{AA} = *body axis components of the aircraft angular velocity*

S_I = *inertial components of the simulator reference – point position*

β_s = *simulator Euler angle*

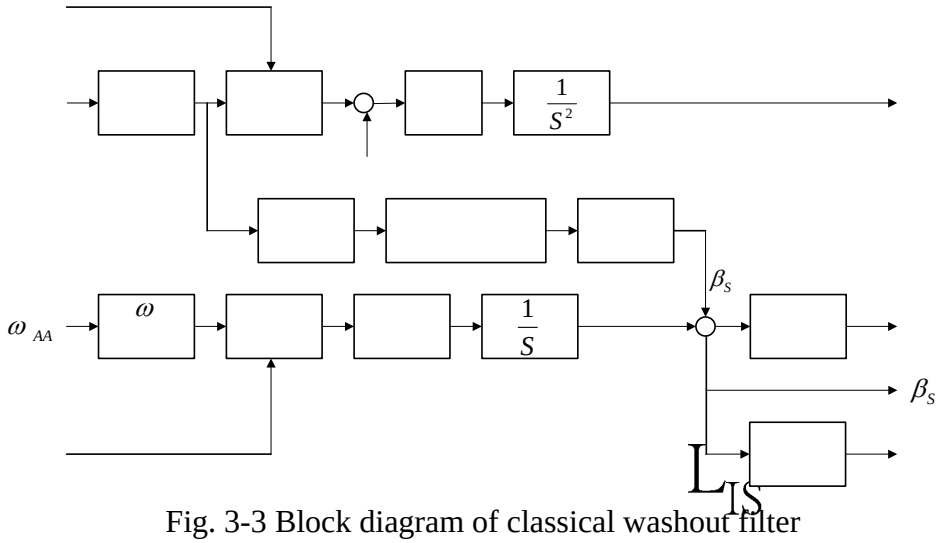

Fig. 3-3 Block diagram of classical washout filter

3.4.1 High-pass specific force channel

As shown in Fig. 3-4, the input is specific force. It is passed through scale, rotation matrix, high-pass filter, etc. As shown in Fig. 3-5, the function of scale block is like nonlinear attenuator introduced in section of human inertial-sensing system. It filters out the specific force which human-beings can't feel. The function of scale block can be formulated as

$$\vec{f}_1 = k(\vec{f}_{AA} - d). \tag{3.4}$$

Then, rotation matrix transforms the vector, $\vec{f}_1$, to inertial frame. And the result is added to gravitational acceleration which is in order to return the gravitational acceleration which is subtracted in the definition of specific force as follows.

$$\vec{f}_3 = L_{IS}\,\vec{f}_1 + \vec{g}_I. \tag{3.5}$$

The function of high-pass filter is to avoid driving the Stewart platform to its limits. Finally, it is integrated twice to obtain the Cartesian position of the payload platform with respect to the base platform.

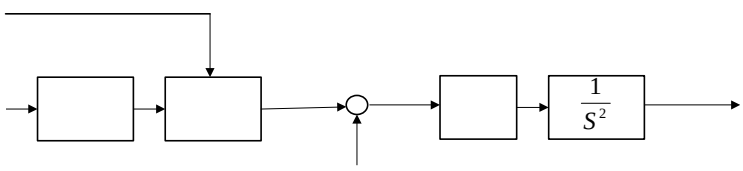

Fig. 3-4 Model of high-pass specific force channel

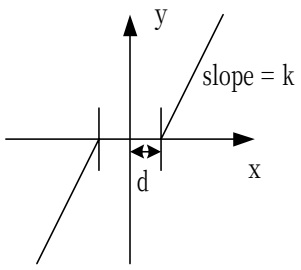

Fig. 3-5 Model of scale

3.4.2 High-pass angular rate channel

The principle of high-pass angular rate channel is like the one of high-pass specific force channel. The model of high-pass angular rate channel is shown in Fig. 3-6. The angular velocity is passed through a scale block to filter out the part that human being can't feel acutely. The function of T_{sx} block is to transform angular velocity to Euler angle rate. Then, it is passed through a high-pass filter to keep the Stewart platform moving within its workspace. Finally, integrate the result to obtain orientation of the payload platform in high frequency part, β_{SH}.

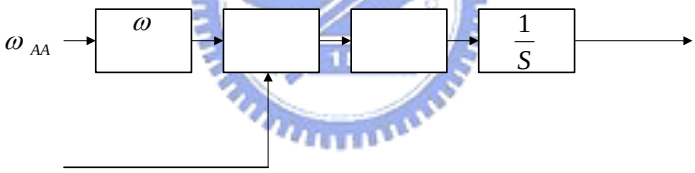

Fig. 3-6 Model of high-pass angular rate channel

3.4.3 Low-pass specific force channel

Because of limited workspace, Stewart Platform can't simulate continuous acceleration for a long time. For human being, we can feel the beginning and the end part of continuous acceleration acutely. These two parts belong to high frequency specific force. And the middle part is usually a uniform acceleration motion and it belongs to low frequency specific force. The purpose of low-pass specific force channel is to simulate the effect of it.

The method of simulating low frequency specific force is to orient the gravity vector in the simulator in the same way relative to the driver as the low-frequency specific force in the vehicle. In this way, it allows sustained acceleration to be simulated. The method is called tilt-coordination and the block diagram is shown in

Fig. 3-7. First, specific force is passed through a scale block and the function of scale block is the same as the one of high-pass specific force channel and high-pass angular rate channel. Then, it is passed through low-pass filter. And tilt-coordination is used to simulate the effect of low-frequency specific force. This trick uses the gravity vector to generate the projection on X-Y plane so it's not available in the vertical direction. As shown in Fig. 3-8, the projections of the gravity vector on X-Y plane can be given as

$$g \cdot \sin(\theta_x) = f_{Ly} \tag{3.6}$$

$$g \cdot \sin(-\theta_y) = f_{Ly}. \tag{3.7}$$

Then, we can obtain

$$\theta_x = \sin^{-1}(\frac{f_{Ly}}{g}) \tag{3.8}$$

$$\theta_y = -\sin^{-1}(\frac{f_{Lx}}{g}) \tag{3.9}$$

$$\theta_z = 0. \tag{3.10}$$

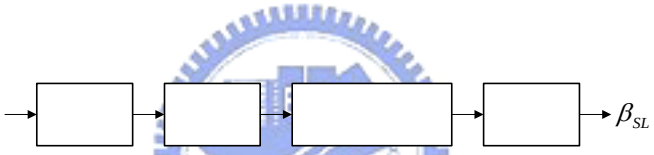

Fig. 3-7 Block diagram of low-pass specific force channel

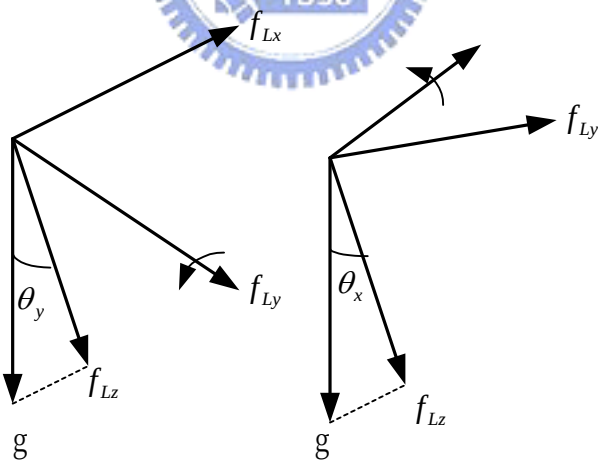

Fig. 3-8 Tile-coordination – rotate around Y and X axis

Finally, it is passed through rate limit block where function limits the angle rate below the threshold value that human being can sense. The typical value is 3 deg/s which is introduced in section 3.3 . The sum of β_{SL} and β_{SH}, the result of low-pass specific force channel and high-pass angular rate channel, is the orientation of the payload platform with respect to the base platform. Therefore, we obtain the Cartesian position and orientation of the payload platform.

3.5 Half-car dynamic model [15] [16] [17]

3.5.1 Motion analysis of x-z plane

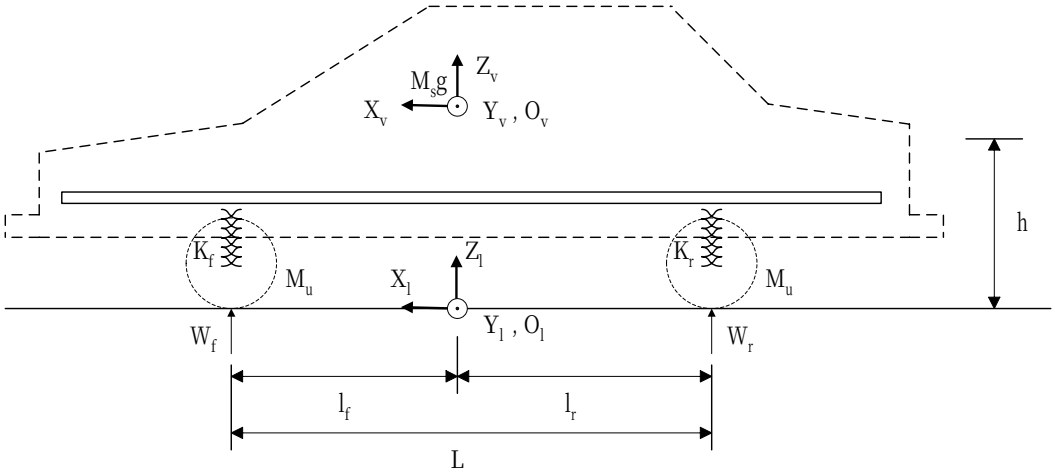

Fig. 3-9 X-Z plane of Half-car dynamic model when stationary or at constant velocity

As shown in Fig.3-9, X_I, Y_I, and Z_I are three axes of global coordinate. X_c , Y_c, and Z_c are three axes of body coordinate where the plane of X_c and Y_c is parallel with the plane of X_I and Y_I. X_c is the forward direction of vehicle. Y_c is the leftward direction of vehicle. X_v, Y_v, and Z_v are three axes of body coordinate. O_c and O_v represent the center of gravity of vehicle. M_s represents the mass of the vehicle and M_u represents the mass of the tire. L and h represent the length between front wheel and rear wheel and the height of the center of gravity of the vehicle, respectively. l_f and l_r represent the length between the center of gravity of the vehicle and front wheel, rear wheel, respectively. K_f and K_r are the spring coefficients of the front and rear suspension system.

When a car is stationary or at a constant velocity, the reactions of the front and rear wheel, W_f and W_r, are

$$W_f = M_u g + M_s g \frac{l_r}{L} \tag{3.11}$$

$$W_r = M_u g + M_s g \frac{l_f}{L}. \tag{3.12}$$

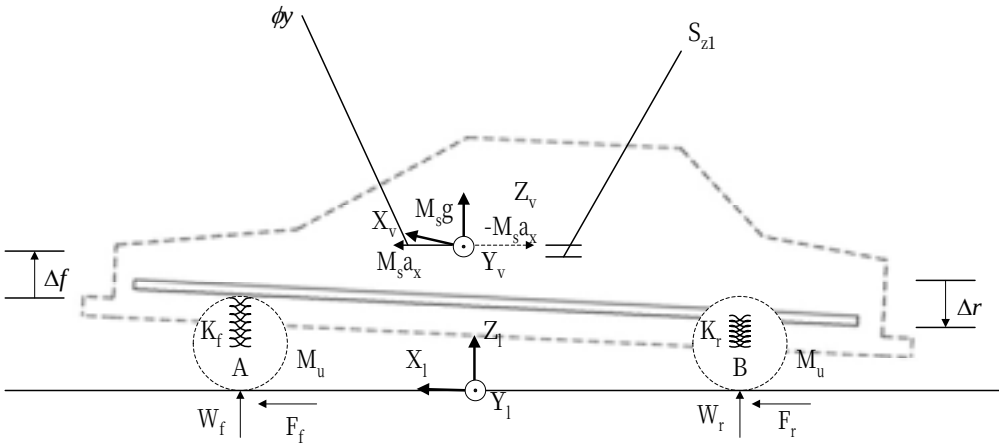

Fig. 3-10 X-Z plane of Half-car dynamic model when accelerating

As shown in Fig. 3-10 F_f and F_r represent front and rear traction on the vehicle. When the car is accelerating at a m/s^2, the total inertia force to the total traction force is given by

$$(M_s + 2M_u)a = F_f + F_r \tag{3.13}$$

Taking moments about point A and B, we can get the reaction force on the rear and front wheel as

$$W_f = M_u g + M_s g \frac{l_r}{L} - \frac{M_s a(h + s_z)}{L} \tag{3.14}$$

$$W_r = M_u g + M_s g \frac{l_f}{L} + \frac{M_s a(h + s_z)}{L} \tag{3.15}$$

where s_z is the deflections along Z axis. The length variations of front and rear suspension system are obtained as

$$\Delta f = \frac{M_s a(h + s_z)}{LK_f} \tag{3.16}$$

$$\Delta r = \frac{M_s a(h + s_z)}{LK_r}. \tag{3.17}$$

Finally, we can obtain the rotation angle of the vehicle along Y axis as

$$\theta y = -\frac{\Delta f + \Delta r}{L}. \tag{3.18}$$

And the deflection of the center of gravity of the vehicle along Z axis is given as

$$s_{z1} = \frac{l_r \Delta f - l_f \Delta r}{L}. \tag{3.19}$$

3.5.2 Motion analysis of y-z plane

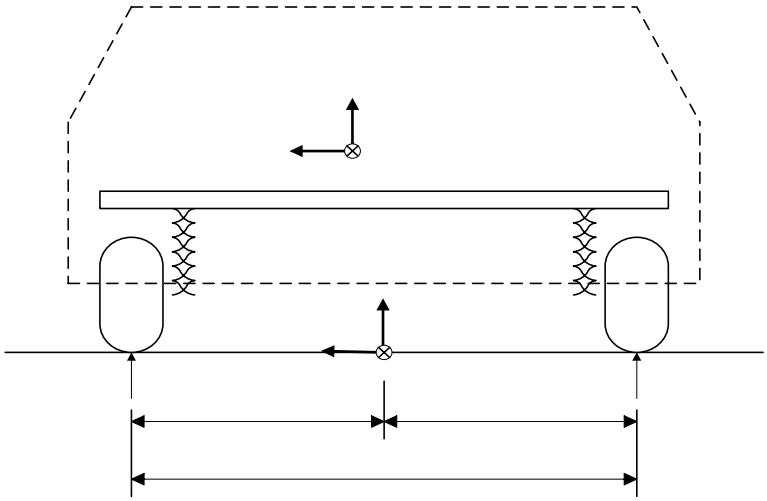

Fig. 3-11 Y-Z plane of Half-car dynamic model when stationary or at constant velocity

As shown in Fig. 3-11, M_s represents the mass of the vehicle and M_u represents the mass of the tire. D represents the length between right wheel and left wheel. d_l and d_{rt} represent the length between the center of gravity of the vehicle and left wheel, right wheel, respectively. K_l and K_{rt} are the spring coefficients of the left and right suspension system. When a car is stationary or at a constant velocity, the reactions of the right and left wheel, W_{rt} and W_l, are

$$W_{rt} = M_u g + M_s g \frac{d_{rt}}{D} \tag{3.20}$$

$$W_l = M_u g + M_s g \frac{d_l}{D}. \tag{3.21}$$

When a car is moving with longitudinal velocity at V_x and yaw rate at $\dot{\theta}_z$ degree/s, the curvature of motion trajectory is given as

$$k = \frac{d\theta_z}{ds} = \frac{\dot{\theta}_z}{V_x}. \tag{3.22}$$

The curvature radius of motion trajectory is given as

$$\rho = \frac{1}{k} = \frac{V_x}{\dot{\theta}_z}. \tag{3.23}$$

According to circular motion theory, we can obtain the acceleration along Y axis as

$$a_y = \frac{Vx^2}{\rho} = V_x \dot{\theta}_z. \tag{3.24}$$

Then, the variation of right and left suspension system can be obtained as

$$F_l + F_{rt} = (M_s + 2M_u)a_y . \tag{3.25}$$

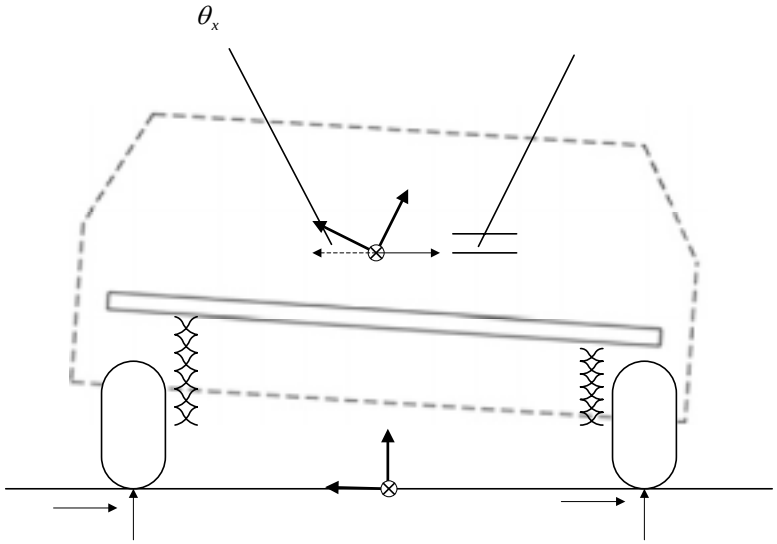

Fig. 3-12 Y-Z plane of Half-car dynamic model when turning right

$$W_l = M_u g + M_s g \frac{d_{rt}}{D} - \frac{M_s a_y (h + s_z)}{D} \tag{3.26}$$

$$W_{rt} = M_u g + M_s g \frac{d_l}{D} + \frac{M_s a_y (h + s_z)}{D} \tag{3.27}$$

$$\Delta_l = \frac{M_s a_y (h + s_z)}{DK_l} \tag{3.28}$$

$$\Delta_{rt} = \frac{M_s a_y (h + s_z)}{DK_{rt}} \tag{3.29}$$

Finally, we can get the rotation angle along X axis, θ_x, and the deflection of the center of gravity of the car along Z axis, Δ_{z2}, as

$$\theta_x = \frac{\Delta_l + \Delta_{rt}}{D} \tag{3.30}$$

$$\Delta_{z2} = \frac{d_{rt}\Delta_l - d_l\Delta_{rt}}{D} \tag{3.31}$$

And, the total deflection of the center of gravity of the vehicle, S_z, is given as

$$S_z = \Delta_{z1} + \Delta_{z2} \tag{3.32}$$

According to this vehicle dynamic model, we can get the acceleration along Y and Z axes and the angle velocity along X and Y axes by inputting the acceleration along X axis and the angle velocity along Z axis. The formulas are given as

$$a_y = \frac{V_x^{\,2}}{\rho} = V_x \dot{\theta}_z \tag{3.33}$$

$$a_z = \frac{d^2 s_z}{dt^2} \tag{3.34}$$

$$\dot{\theta}_x = \frac{d\theta_x}{dt} \tag{3.35}$$

$$\dot{\theta}_y = \frac{d\theta_y}{dt}. \tag{3.36}$$

From section 3.5.1 and 3.5.2, we get the linear acceleration and angle velocity along X, Y, and Z axes respect to global coordinate. However, pilot is taken specific force under non-inertial coordinate. We need to transform the linear acceleration and angle velocity with respect to inertial coordinate into specific force that pilot is taken with respect to non-inertial coordinate. Here, three coordinates are defined. One is inertial coordinate (X_I, Y_I, and Z_I), one is moving coordinate system (X_v, Y_v, and Z_v) at the center of gravity of vehicle as shown in Fig. 3-9 to Fig. 3-12, and one is moving coordinate at the driver seat (X_A, Y_A, and Z_A). Let $\vec{q}_{VA}^{\,I}$ represent the vector between the driver seat and the center of gravity of vehicle respect to inertial coordinate. There is no relative displacement between the driver seat and the center of gravity of vehicle. So, $\dot{\vec{q}}_{VA} = \ddot{\vec{q}}_{VA} = 0$. We can obtain [18]

$$\vec{q}_{IA}^{\,I} = \vec{q}_{IV}^{\,I} + \vec{q}_{VA}^{\,I} \tag{3.37}$$

and

$$\dot{\vec{q}}_{VA}^{\,I} = \vec{\omega}_{IV}^{\,I} \times \vec{q}_{VA}^{\,I}. \tag{3.38}$$

And a cross product on left side by a vector is equivalent to pre-multiplication by its skew-symmetric matrix form. $\dot{\vec{q}}_{VA}^{\,I}$ is given by [18]

$$\dot{\vec{q}}_{VA}^{\,I} = \Omega_{IV}^{I} \cdot \vec{q}_{VA}^{\,I} \tag{3.39}$$

where

$$\Omega_{IV}^{I} = \begin{bmatrix} 0 & -\omega_{IV3}^{I} & \omega_{IV2}^{I} \\ \omega_{IV3}^{I} & 0 & -\omega_{IV1}^{I} \\ -\omega_{IV2}^{I} & \omega_{IV1}^{I} & 0 \end{bmatrix}. \tag{3.40}$$

From equation 3.37, $\dot{\vec{q}}_{IA}^{\,I}$ can be obtained as [18]

$$\dot{\vec{q}}_{IA}^{\,I} = \dot{\vec{q}}_{IV}^{\,I} + \dot{\vec{q}}_{VA}^{\,I} = \dot{\vec{q}}_{IV}^{\,I} + R_V^I(\dot{\vec{q}}_{VA}^{\,V} + \Omega_{IV}^{V} \cdot \vec{q}_{VA}^{\,V}) \tag{3.41}$$

and

$$\ddot{\vec{q}}_{IA}^{I} = \ddot{\vec{q}}_{IV}^{I} + R_V^I(\ddot{\vec{q}}_{VA}^{V} + \dot{\Omega}_{IV}^{V} \cdot \vec{q}_{VA}^{V} + 2\Omega_{IV}^{V} \cdot \dot{\vec{q}}_{VA}^{V} + \Omega_{IV}^{V} \cdot \Omega_{IV}^{V} \cdot \vec{q}_{VA}^{V}) . \quad (3.42)$$

where matrix R_V^I represents the transformation matrix from moving coordinate (X_v, Y_v, and Z_v) to inertial coordinate (X_I, Y_I, and Z_I) and $\dot{\vec{q}}_{IA}^{I}$ is the first differential of $\vec{q}_{IA}^{I}$. Multiply equation 3.42 by R_I^V and we can transform $\ddot{\vec{q}}_{IA}^{I}$ from inertial coordinate into moving coordinate (X_v, Y_v, and Z_v)

$$R_I^V \cdot \ddot{\vec{q}}_{IA}^{I} = R_I^V \cdot \ddot{\vec{q}}_{IV}^{I} + (\ddot{\vec{q}}_{VA}^{V} + \dot{\Omega}_{IV}^{V} \cdot \vec{q}_{VA}^{V} + 2\Omega_{IV}^{V} \cdot \dot{\vec{q}}_{VA}^{V} + \Omega_{IV}^{V} \cdot \Omega_{IV}^{V} \cdot \vec{q}_{VA}^{V}) . \quad (3.43)$$

Chapter 4

Simulation with Hydraulic Systems

4.1 Simulation blocks

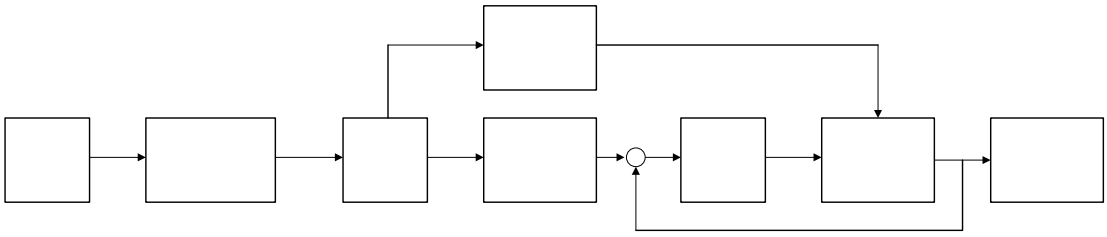

Fig. 4-1 The block diagram of a simulation system

The complete block diagram of simulation system is shown in Fig. 4-1. First, the forward acceleration and angular rate of vehicle are the inputs of car dynamic model and linear acceleration and angular rate of center of gravity of vehicle along X, Y and Z axes with respect to global coordinate are given. However, the specific force that driver experiences, the input of washout filter, happens when car is moving. It is a non-inertial coordinate. We need to transform the global coordinate into non-inertial coordinate with a point in car as reference point. The driver seat is selected. After transformation, the specific force is passed into washout filter and motion trajectory of Stewart platform is given. Then, the corresponding lengths of six actuators and the force of each actuator are derived by inverse kinematics and inverse dynamics. Next, we transform the length of the actuator into the corresponding current signal. The force given by inverse dynamics is the input of electro-hydraulic system. The hydraulic system is controlled by PID controller to reach the desired position. Finally, we use forward kinematics to transform the length of six actuators into Cartesian position and orientation of the Stewart Platform.

car dynamic model

Coordinate transformation

4.2 The electro-hydraulic system [19]

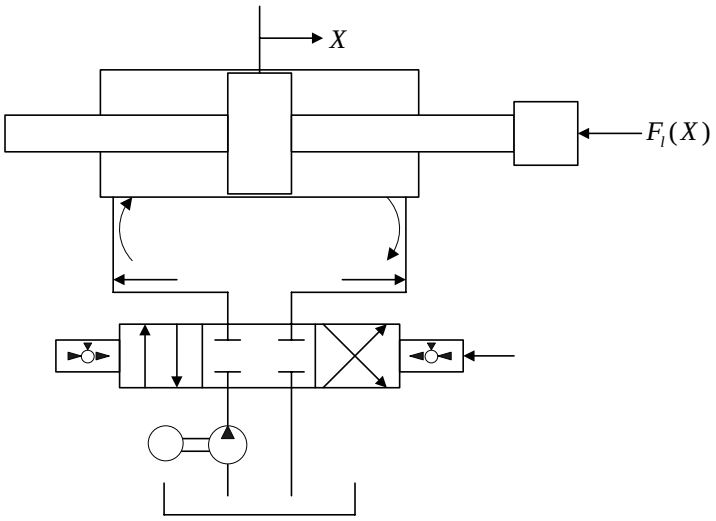

Fig. 4-2 Schematic diagram of electro-hydraulic control system

As shown in Fig. 4-2, the pump converts its energy of rotation into a flow. The flow is usable to the output device, hydraulic actuator. The relief valve sets a maximum pressure value in the system. When the pressure value exceeds the maximum value, oil is dumped to the tank to relieve the pressure. The servo valve controls or changes the flow into the hydraulic actuator. The input of the servo valve is current, i. From orifice law the load flow rate Q_I of the servo valve is given by

$$Q_I = Ki\sqrt{P_s - \text{sgn}(i)P_l} \tag{4.1}$$

where the input current i is limited by maximum input current $i_{\max}$

$$|i| \le i_{\max}. \tag{4.2}$$

P_l is the load pressure across the cylinder. Let A be the piston ram area, C_t be the total leakage coefficient, V_t be the total volume of the valve and the cylinder chamber, β be the bulk modulus of the oil and $\dot{X}$ be the velocity of the piston. According to the continuity equation of the servo valve and cylinder chamber, we can obtain the formula as

$$Q_I = A\dot{X} + C_t P_l + (\frac{V_t}{4\beta})P_l. \tag{4.3}$$

And if we neglect the Coulomb friction between the piston and its sleeve, we can obtain the equation of motion of the piston as

$$AP_l = M\ddot{X} + B\dot{X} + F \tag{4.4}$$

where B is the viscous damping coefficient, F is the external load disturbance which can be obtained from inverse dynamics.

4.3 Simulation results

Case 1：

Forward acceleration is 5 m/s^2 and it lasts for 4 seconds. Then forward acceleration decreases to 0 in one second. As shown in Fig. 4-3, yaw rate is zero. Fig. 4-3 and Fig. 4-4 show the response of linear acceleration and angular rate of center of gravity of vehicle along each axis with respect to global coordinate.

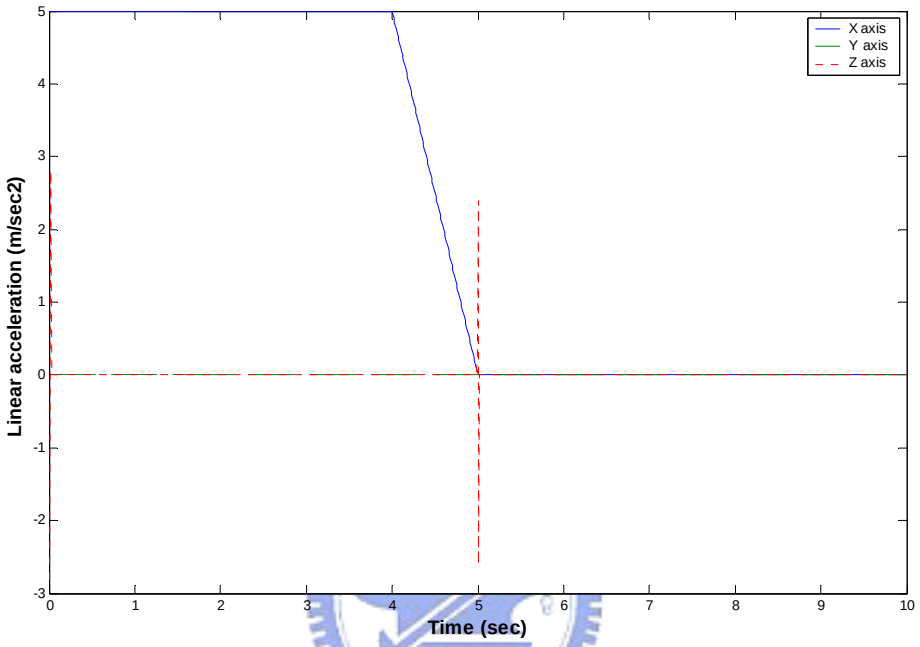

Fig.4-3 Linear acceleration along x, y, and z axis

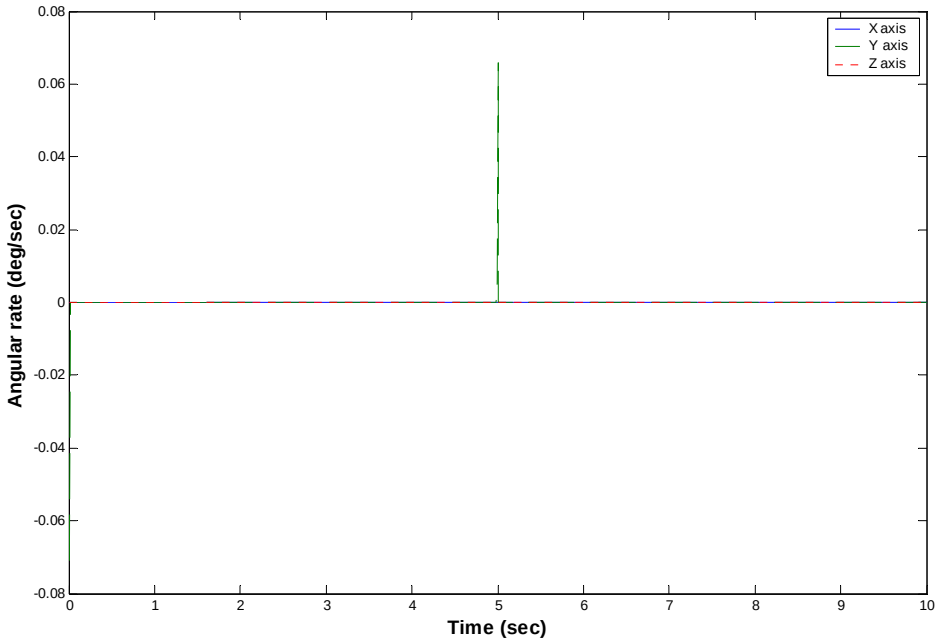

Fig.4-4 Angular rate along x, y, and z axis

Once we make sure of the driving situation, we get the position and orientation of Stewart platform through coordinate transformation and washout filter. Then, we can get the corresponding length of each actuator by inverse kinematics. The simulation results are shown in Fig.4-7 and Fig. 4-8. They also include the real response of each actuator. Next, we can get the force of each actuator by inverse dynamics. The simulation results are shown in Fig. 4-5 and Fig. 4-6.

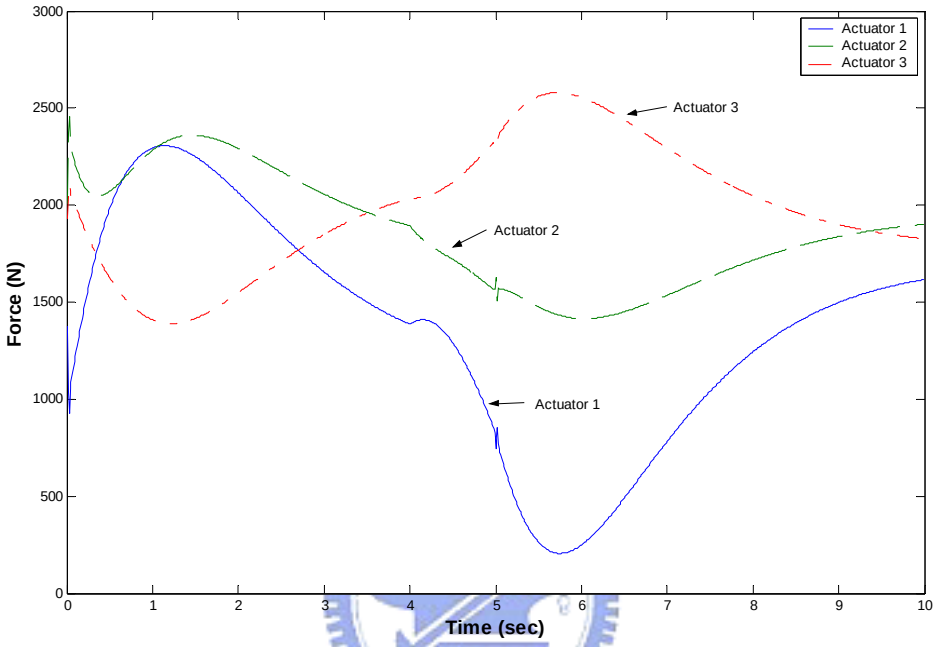

Fig.4-5 The force of actuator1, 2 and 3

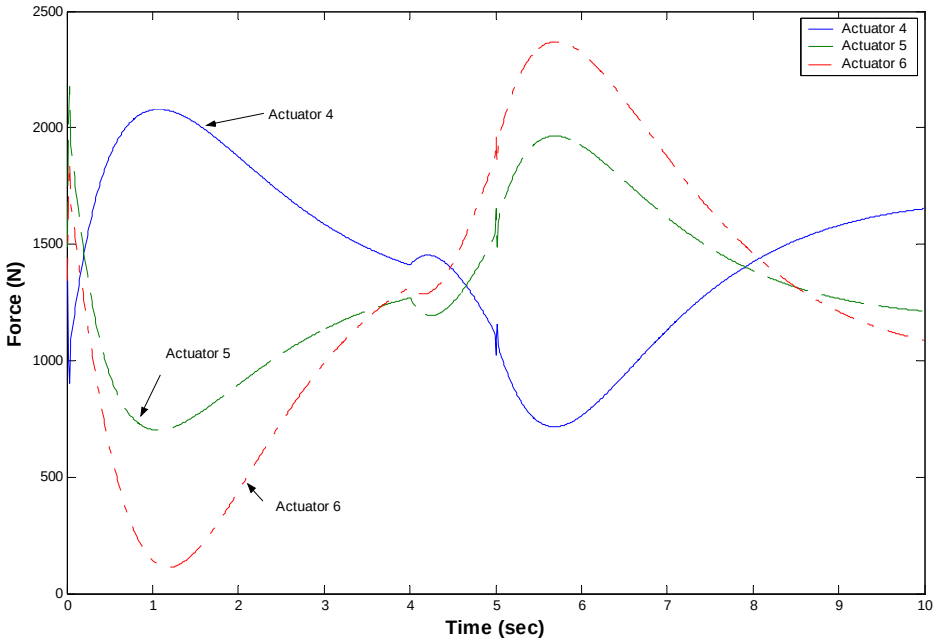

Fig.4-6 The force of actuator 4, 5 and 6

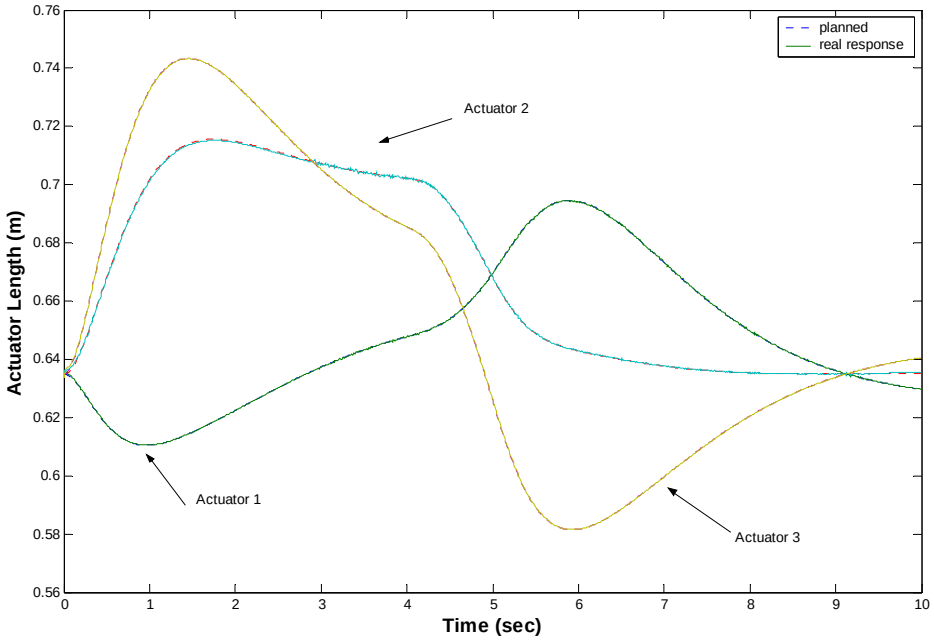

Fig.4-7 The length of actuator 1, 2, and 3

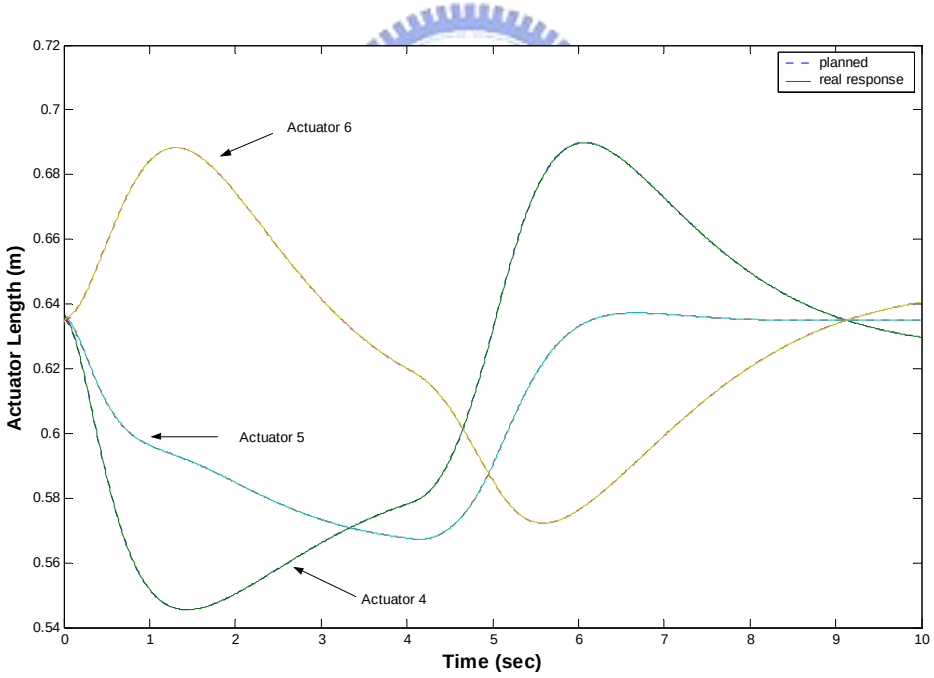

Fig.4-8 The length of actuator 4, 5, and 6

From Fig.4-7 and Fig.4-8, we can obtain the length errors of six actuators which are shown in Fig.4-9 to Fig.4-10. The simulation results show that the length error of each actuator is below 2 millimeter.

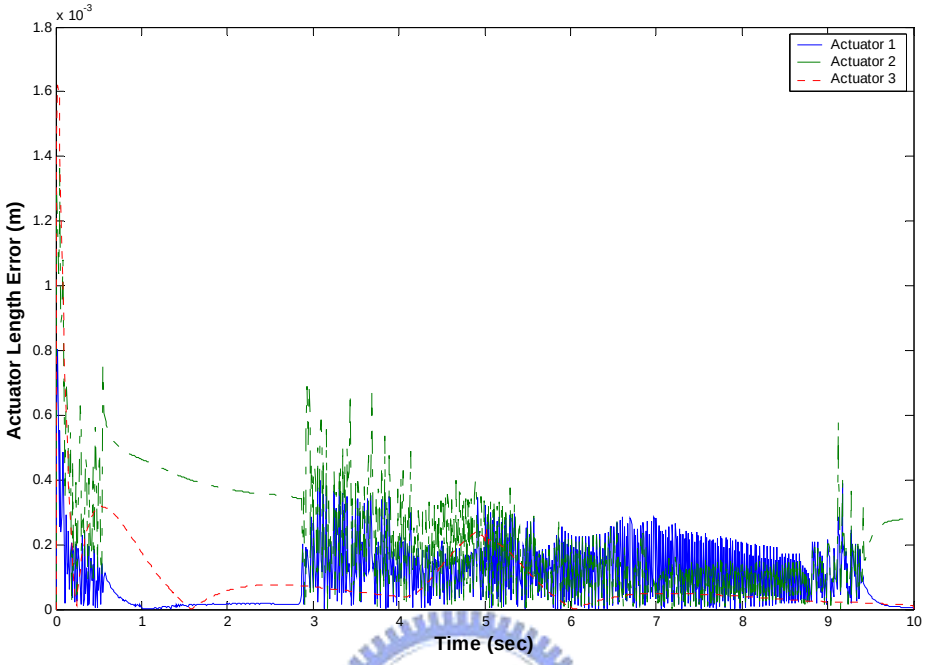

Fig.4-9 The length error of actuator 1, 2 and 3

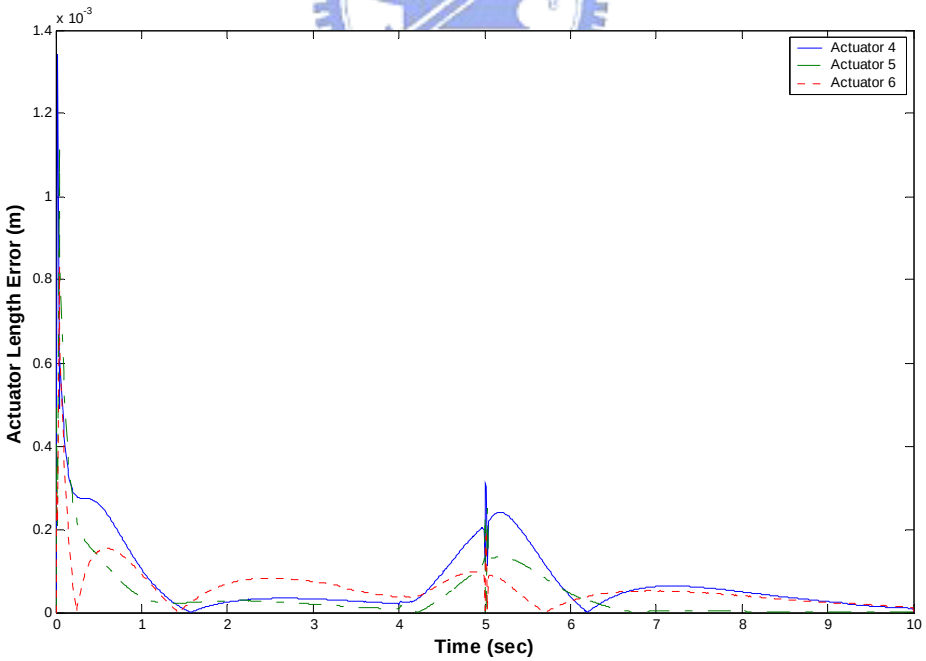

Fig.4-10 The length error of actuator 4, 5 and 6

Finally, Fig. 4-11 through Fig. 4-16 show the results when we use forward kinematics to transform the real lengths of six actuators into corresponding position and orientation of Stewart platform. In Fig. 4-11, we see that the platform moves forward about 0.11 meter and is pulled back to the initial position. The purpose of this trajectory is to give the pilot the feeling of moving forward and keep the platform in maximum workspace. When linear acceleration is decreasing, the platform moves backward to do the same thing.

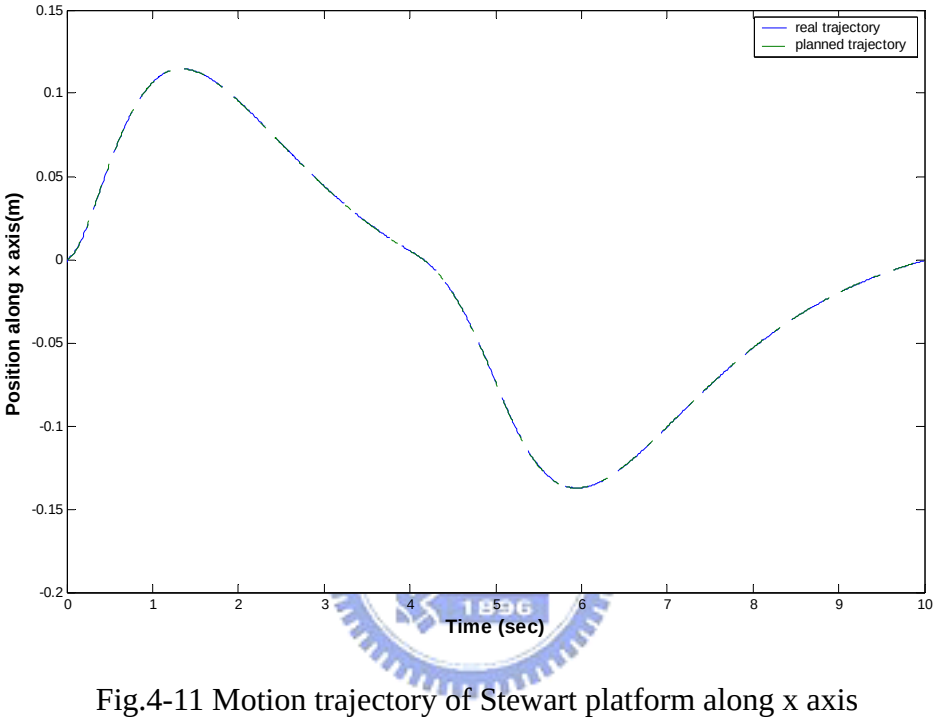

Fig.4-11 Motion trajectory of Stewart platform along x axis

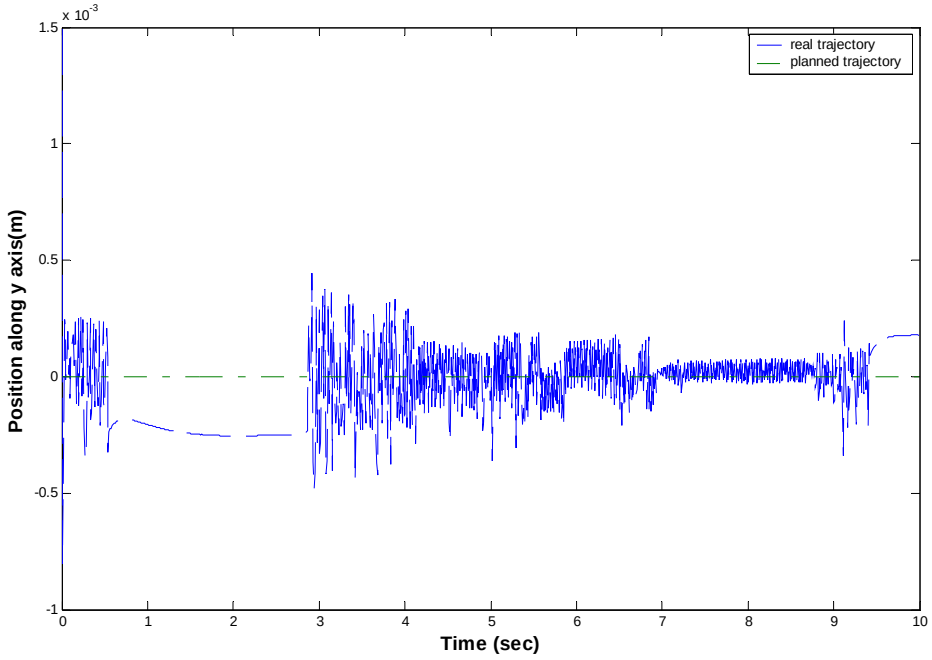

Fig.4-12 Motion trajectory of Stewart platform along y axis

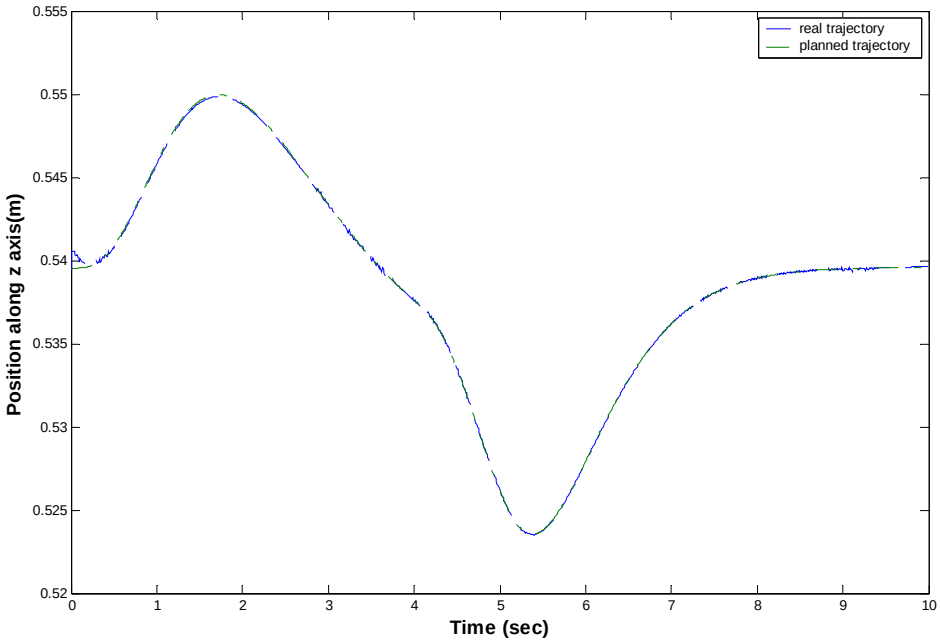

Fig.4-13 Motion trajectory of Stewart platform along z axis

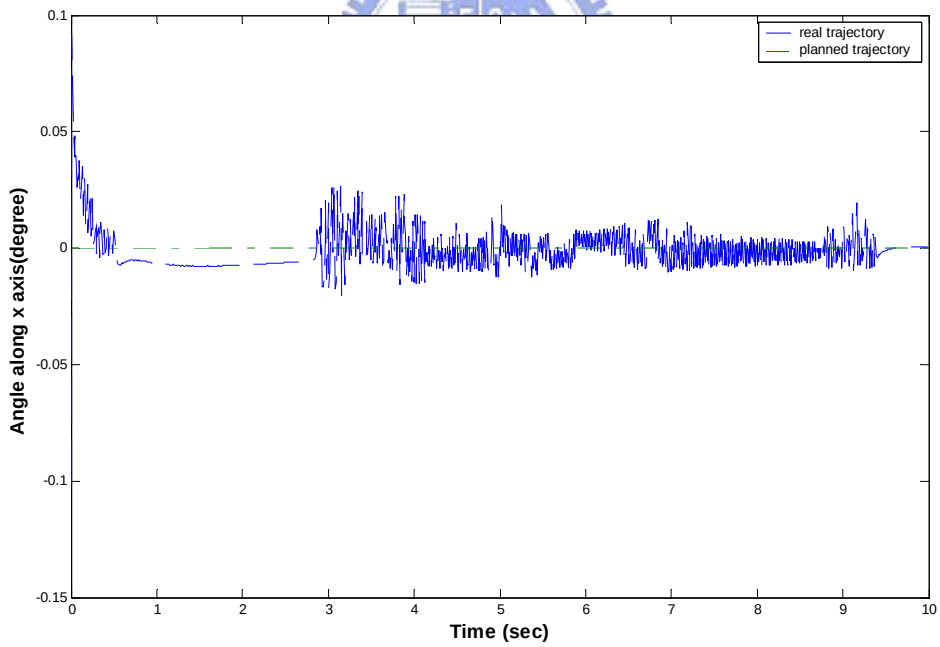

Fig.4-14 Rotation angle of Stewart platform along x axis

In Fig. 4-15, we can see that the angle along y axis (pitch) is about -11 degrees and lasts for 3 seconds. In this trajectory, the car keeps doing the motion of linear acceleration. In order to let the pilot feels realistic, the platform rotates and uses gravity to give the pilot the corresponding specific force. When the motion of linear acceleration disappears, the platform rotates to its initial posture.

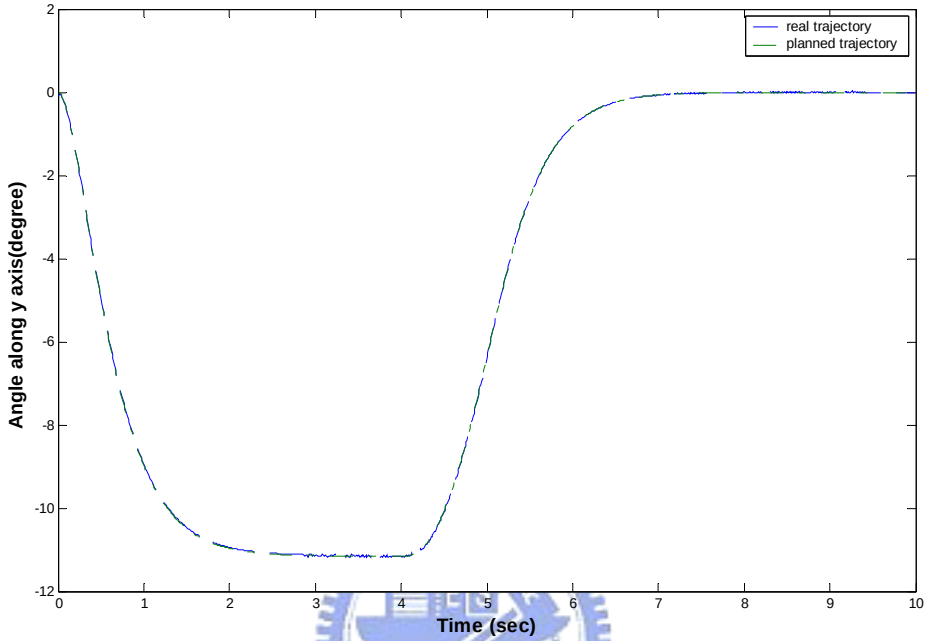

Fig.4-15 Rotation angle of Stewart platform along y axis

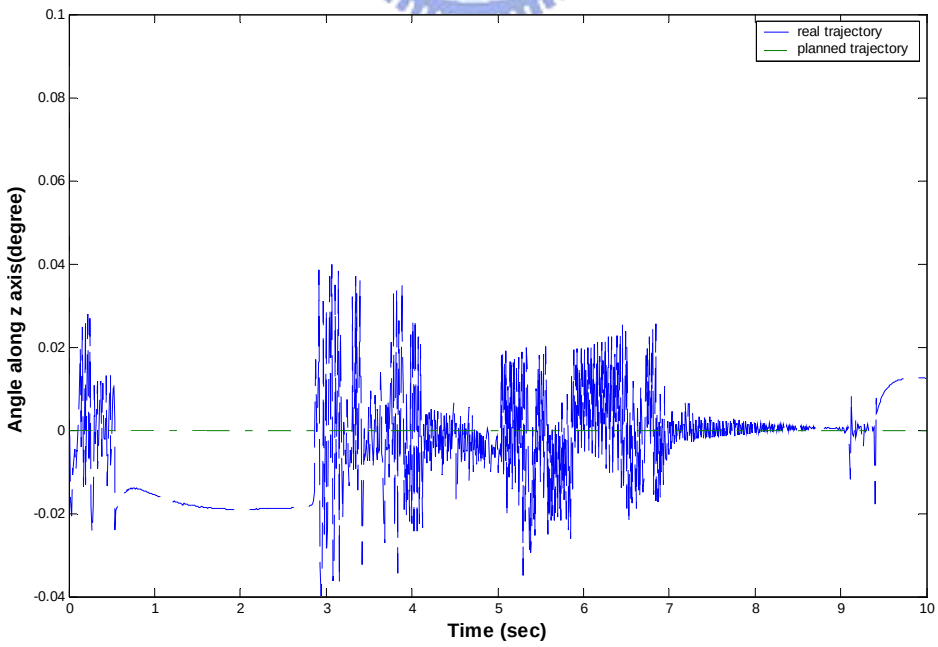

Fig.4-16 Rotation angle of Stewart platform along z axis

Fig. 4-17 and Fig. 4-18 show the errors of position and orientation of motion trajectory. From Fig. 4-17, the position errors along x, y, and z axes are below 1.5 millimeter. And the rotation angle errors along three axes are below 0.15 degree.

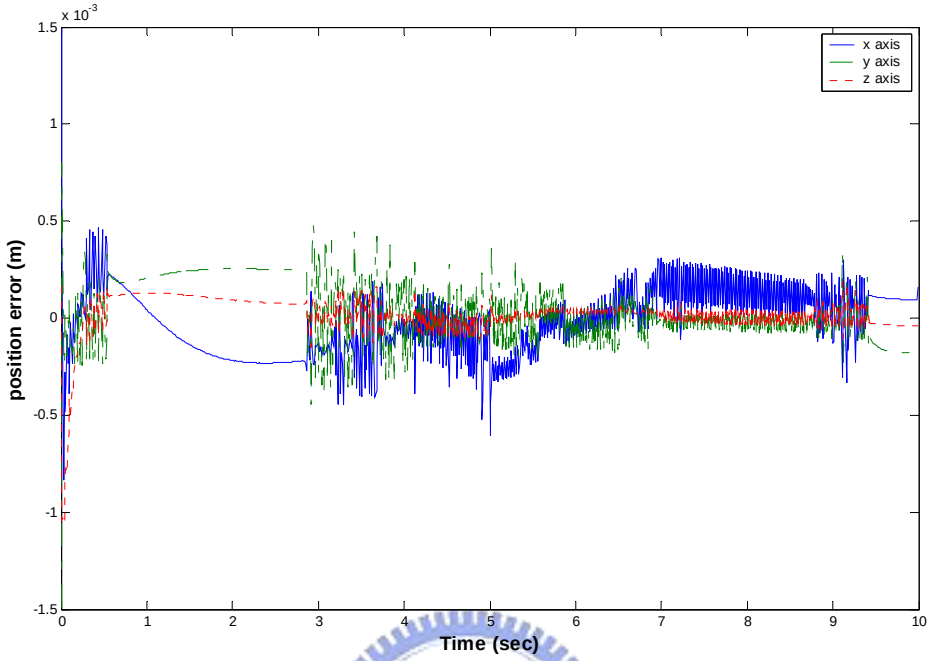

Fig.4-17 Position error of motion trajectory

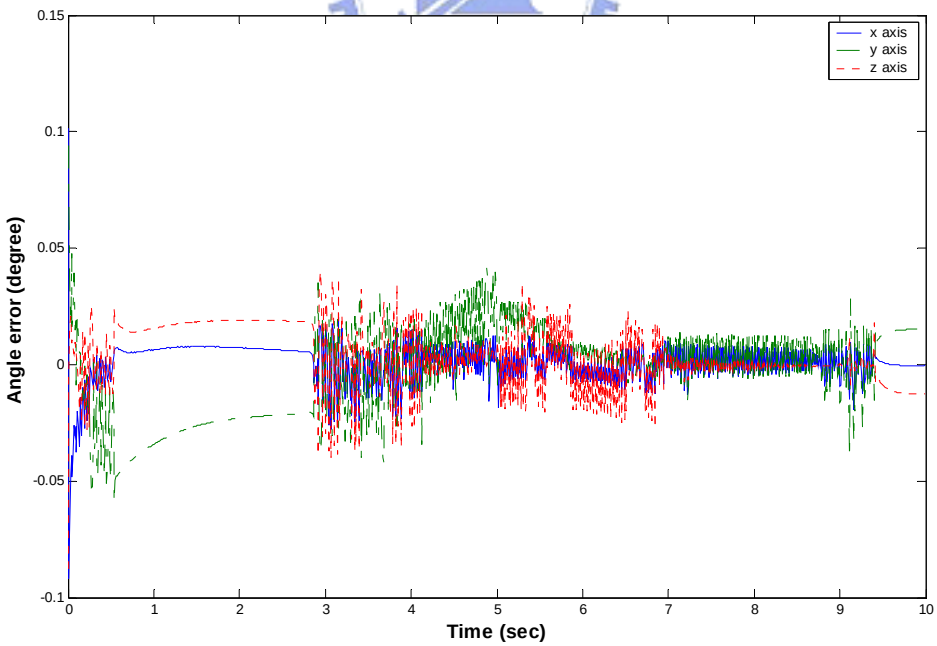

Fig.4-18 Rotation angle error of motion trajectory

Case 2：

The second simulation case is that a car moves forward and turns left at the same time. Fig. 4-19 and Fig. 4-20 show the linear acceleration and angular rate of center of gravity of vehicle along each axis with respect to global coordinate. Forward acceleration is 5 m/s^2 and it lasts for 4 seconds. Then forward acceleration decreases to 0 in one second. As shown in Fig. 4-20 yaw rate is 0.15 and it lasts for 4 seconds. Then yaw rate decreases to 0 in one second.

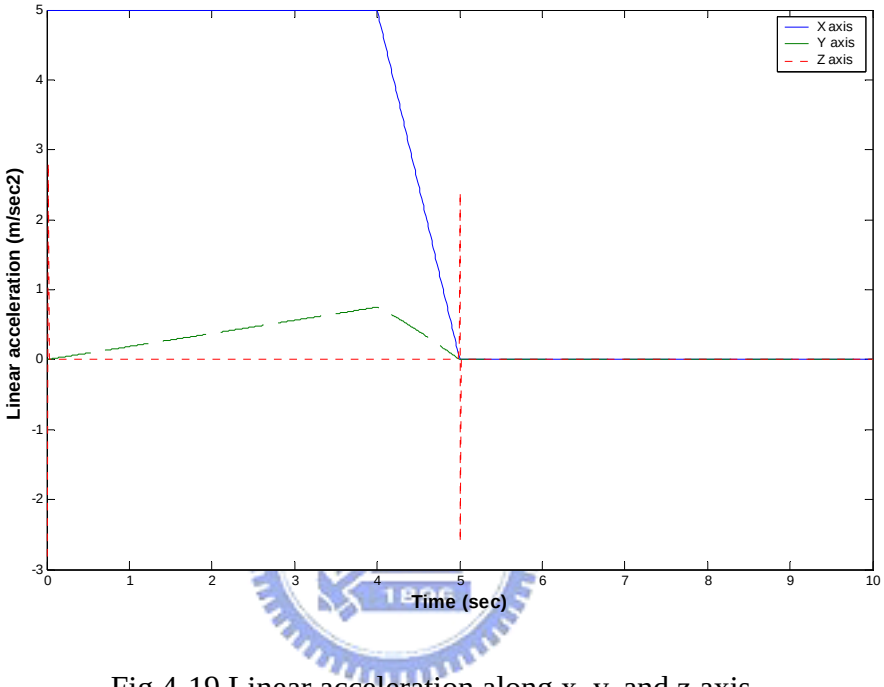

Fig.4-19 Linear acceleration along x, y, and z axis

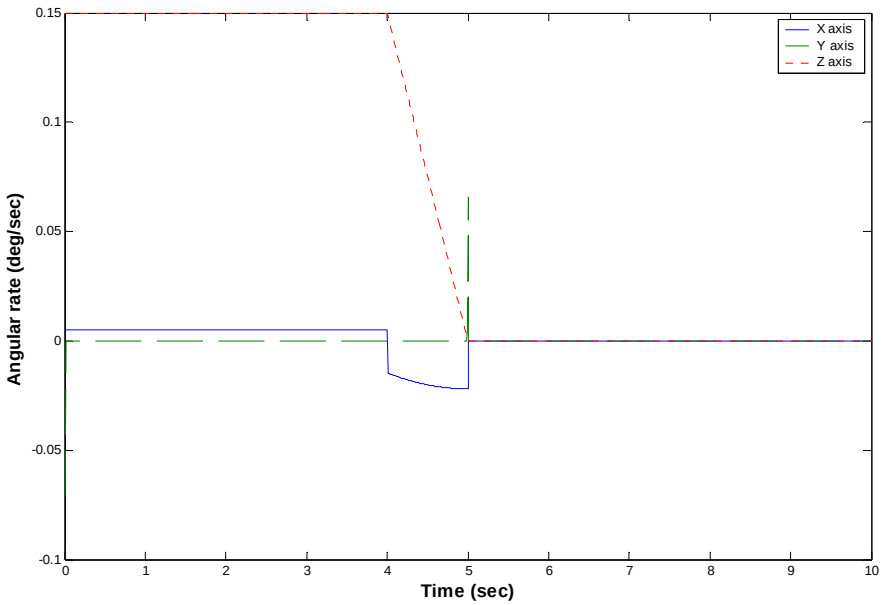

Fig.4-20 Angular rate along x, y, and z axis

Once we get the linear acceleration and angular rate of center of gravity of vehicle, we can obtain the corresponding motion trajectory of Stewart platform through coordinate transformation and washout filter. Then, the length of each actuator is given by inverse kinematics. The simulation results shown in Fig.4-23 and Fig.4-24 are the corresponding lengths of six actuators. Besides, the force of each actuator are shown in Fig. 4-21 and Fig. 4-22.

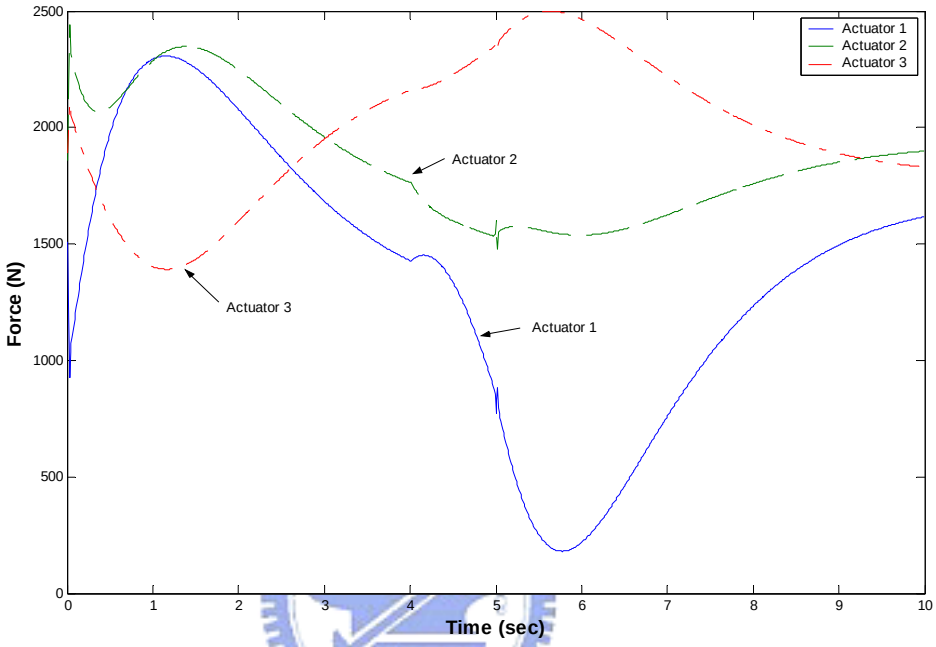

Fig.4-21 The force of actuator 1, 2, and 3

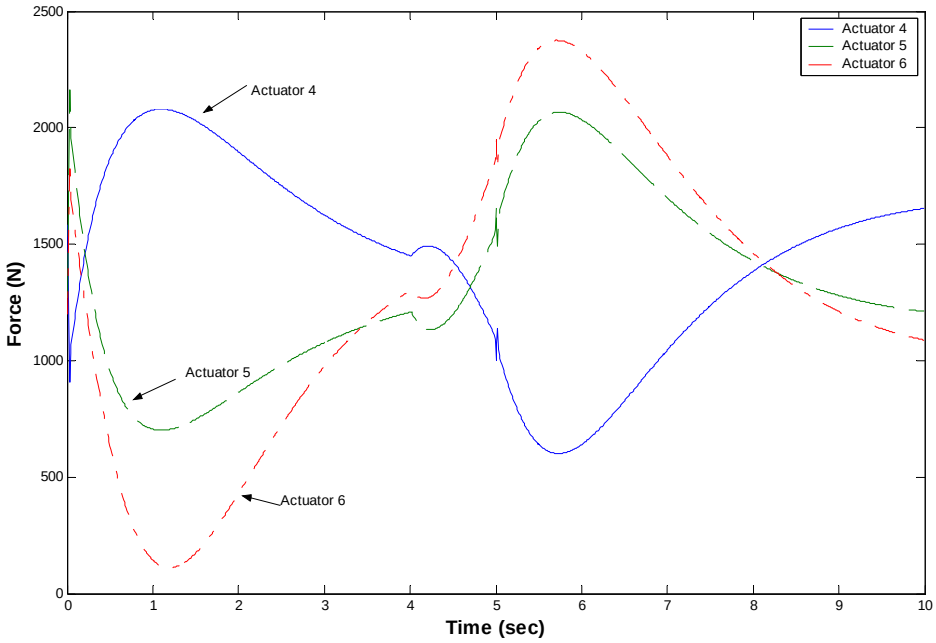

Fig.4-22 The force of actuator 4, 5, and 6

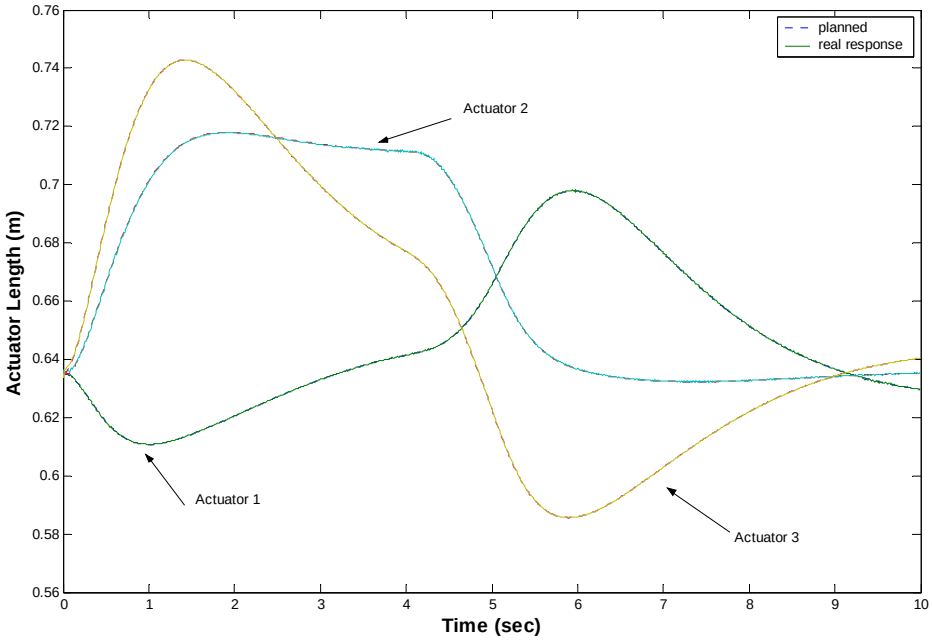

Fig.4-23 The length of actuator 1, 2, and 3

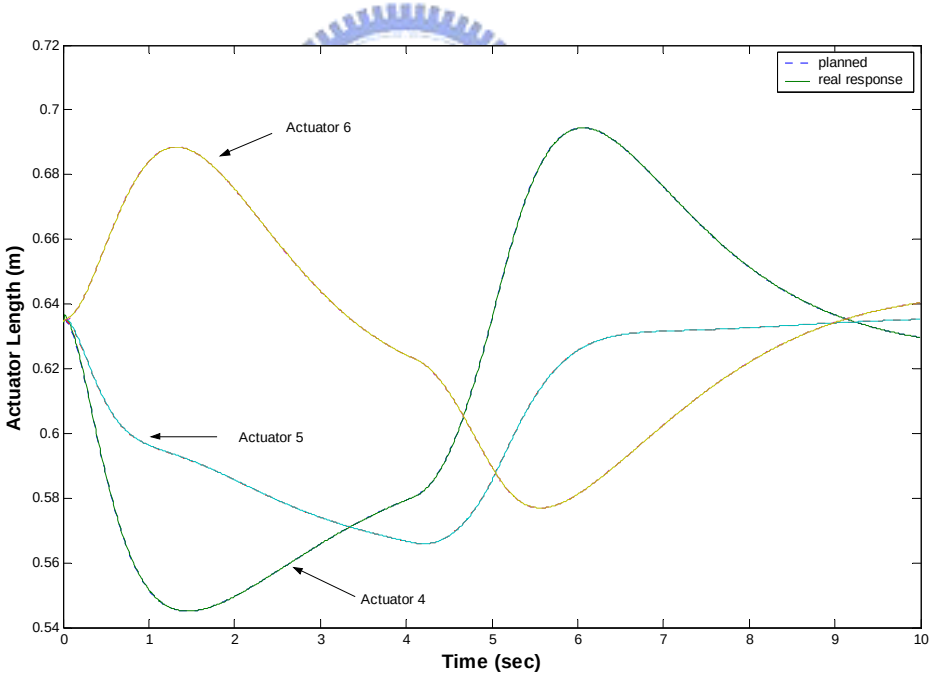

Fig.4-24 The length of actuator 4, 5, and 6

From Fig. 4-23 and Fig. 4-24, we can obtain the length errors of six actuators which are shown in Fig.4-25 and Fig.4- 26. The simulation results show that the length error of each actuator is below 1.6 millimeter.

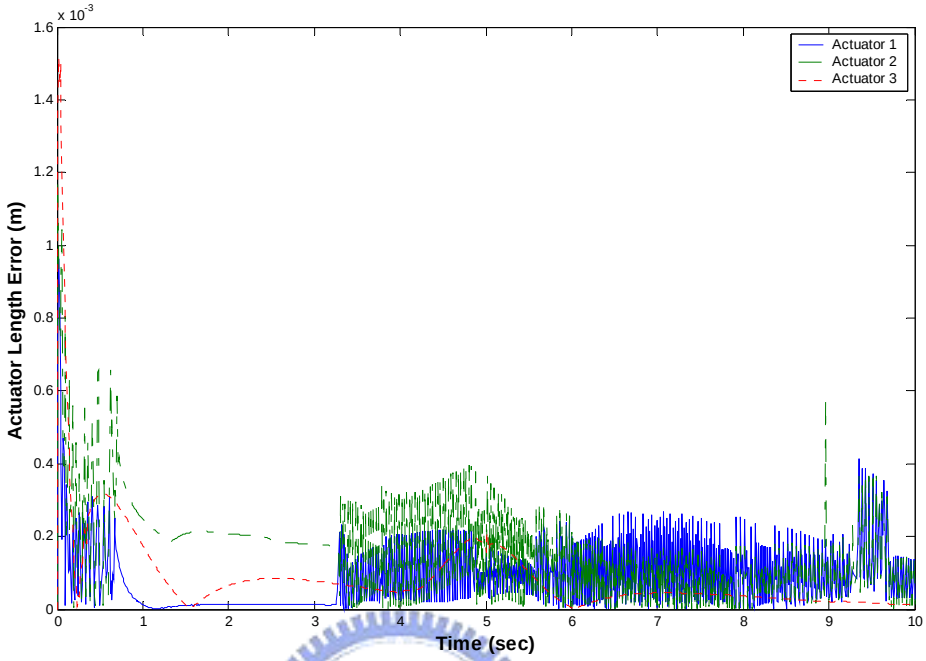

Fig.4-25 The length error of actuator 1, 2, and 3

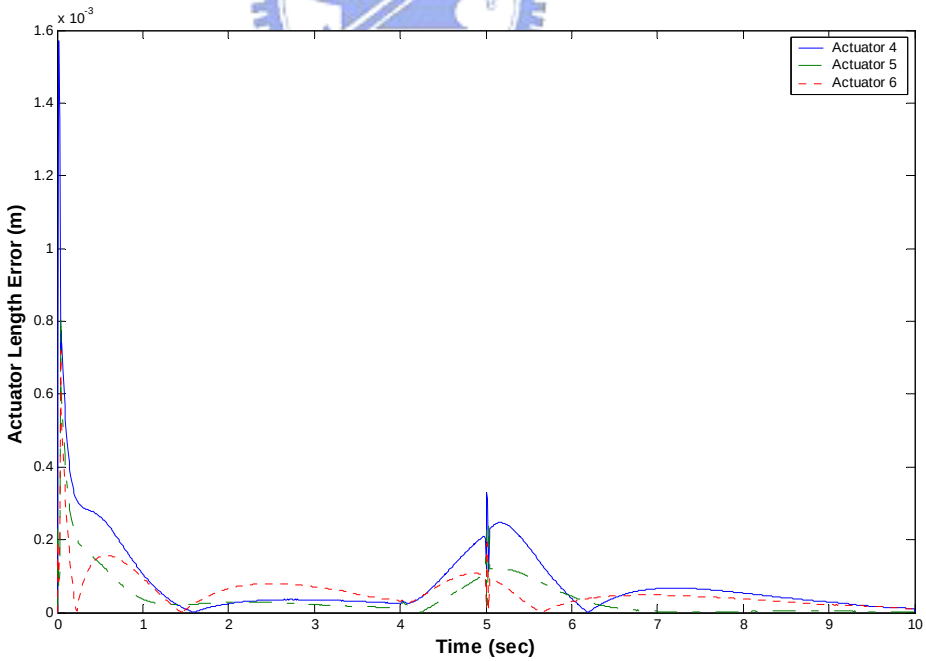

Fig.4-26 The length error of actuator 4, 5, and 6

Finally, Fig. 4-27 through Fig. 4-32 show the results that we use forward kinematics to transform the actual lengths of six actuators into corresponding position

and orientation of Stewart platform. From Fig. 4-27, we see that the platform moves forward about 0.11 meter and is pulled back to the initial position. The purpose of this trajectory is to give the pilot the feeling of moving forward and keep the platform in maximum workspace. However, the car turns left at the same time. From Fig. 4-32, we can see that the platform rotates along z axis until yaw rate is zero. The simulation results are pretty conform the driving situation.

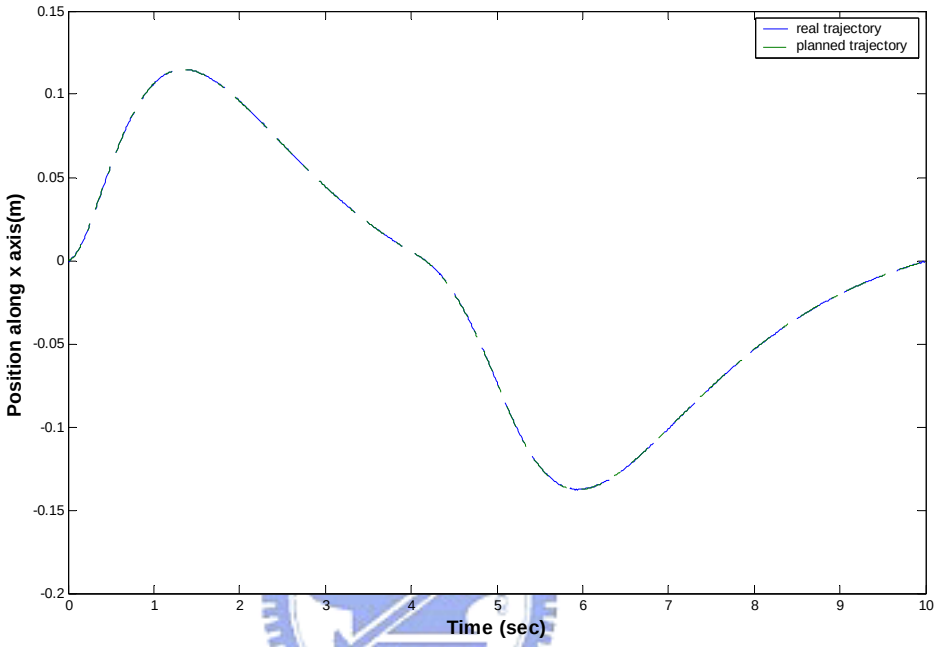

Fig.4-27 Motion trajectory of Stewart platform along x axis

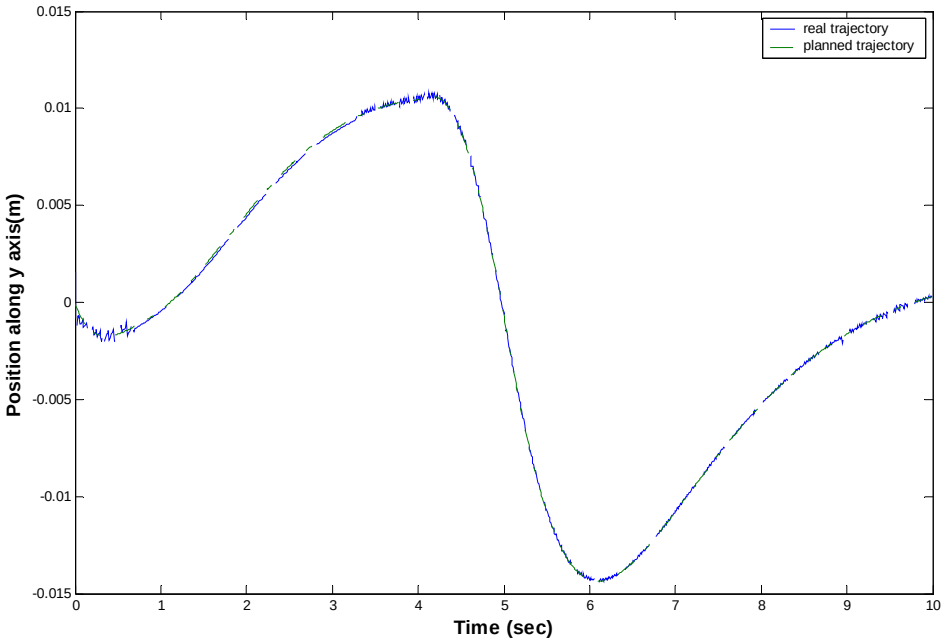

Fig.4-28 Motion trajectory of Stewart platform along y axis

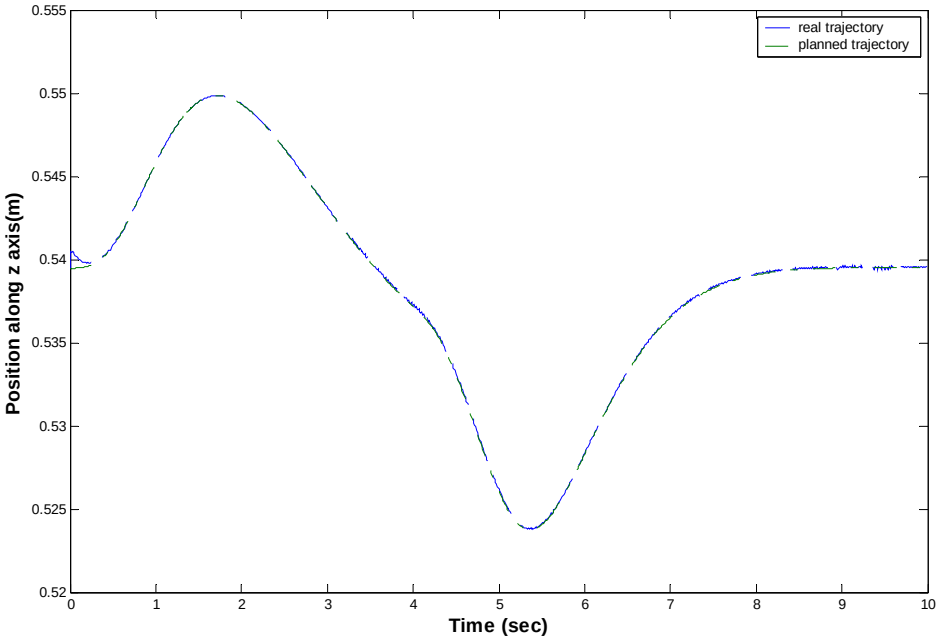

Fig.4-29 Motion trajectory of Stewart platform along z axis

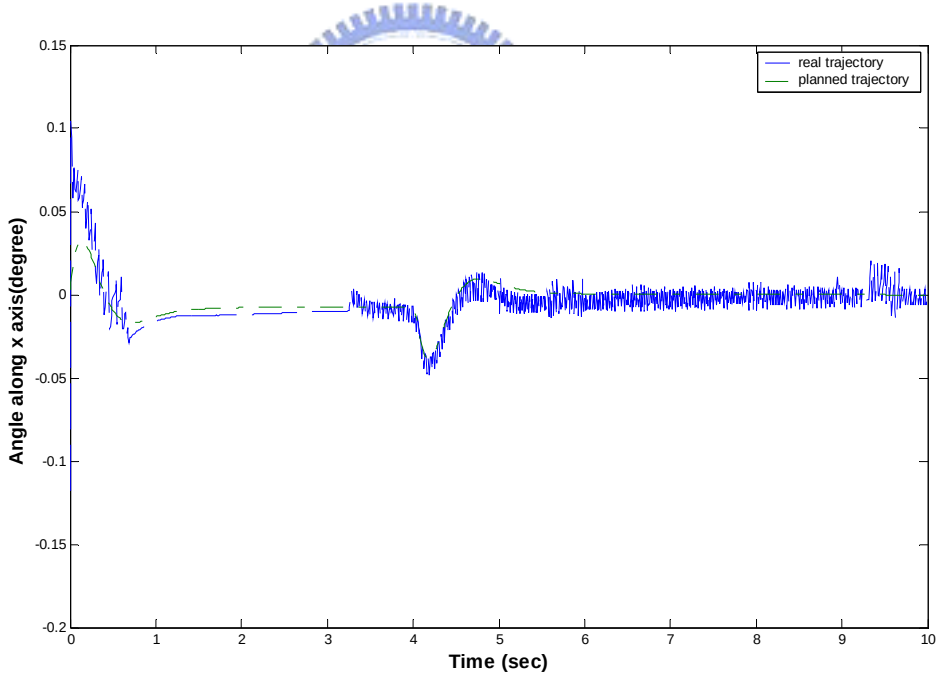

Fig.4-30 Rotation angle of Stewart platform along x axis

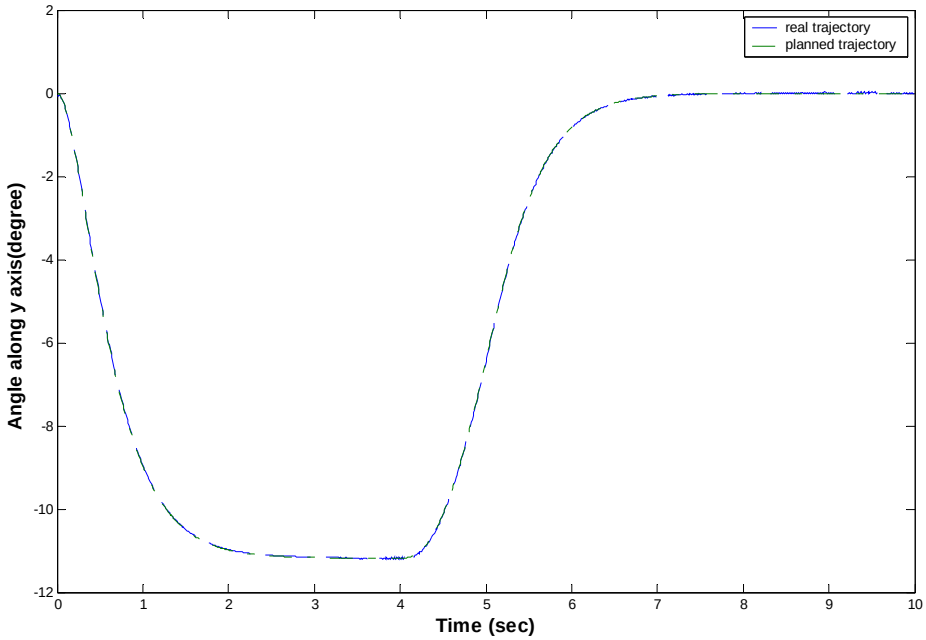

Fig.4-31 Rotation angle of Stewart platform along y axis

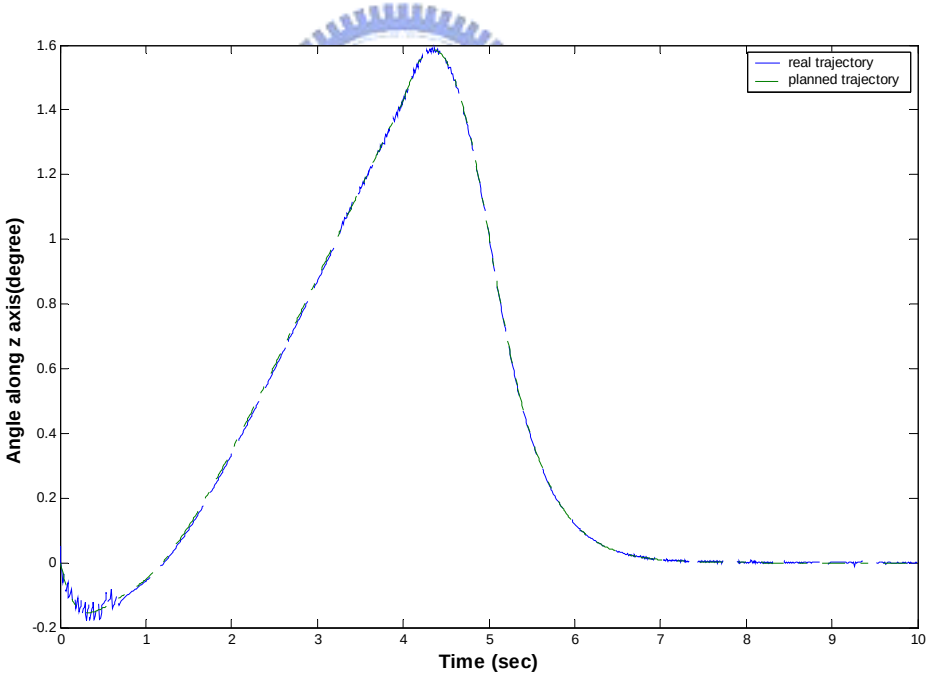

Fig.4-32 Rotation angle of Stewart platform along z axis

Fig. 4-33 and Fig. 4-34 show the errors of position and orientation of motion trajectory. From Fig. 4-33, the position errors along x, y, and z axes are below 1.5 millimeter. And the orientation errors along each axis are below 0.15 degree.

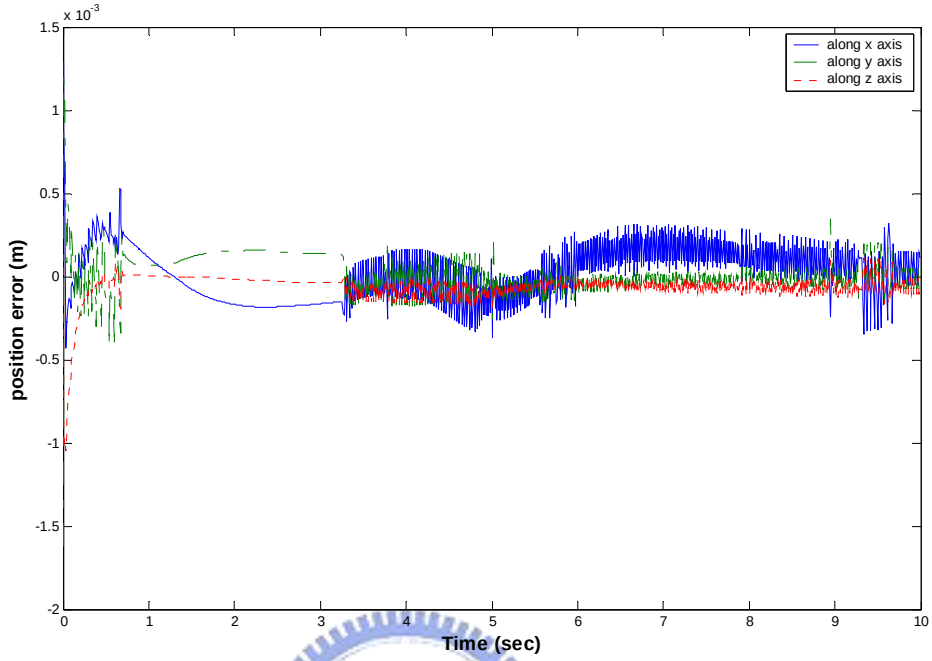

Fig.4-33 Position error of motion trajectory

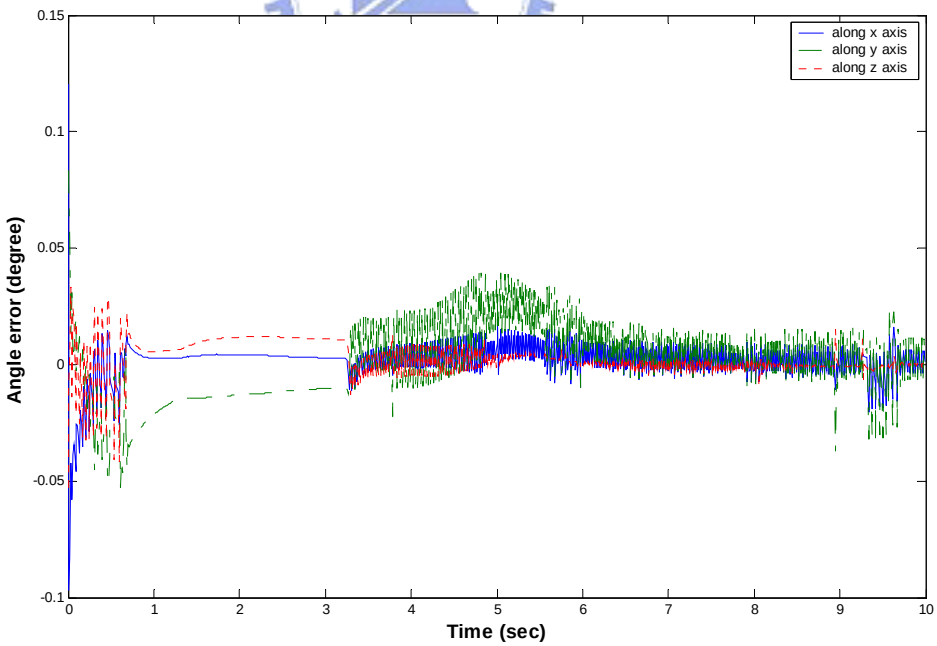

Fig.4-34 Rotation angle error of motion trajectory

Chapter 5

Conclusions

In this thesis, we have analyzed a simulator based on Stewart platform. First, a car dynamic model was obtained and it was made sure of what kind of driving situation to be simulated. Then, we could obtain linear acceleration and angular rate of the center of gravity of the vehicle along x, y, and z axes. Using dynamics in non-inertial coordinates, force of a reference point in car was given. It was passed into washout filter and trajectory of Stewart platform was obtained. The force that each actuator has to be taken, external disturbance, is known by inverse dynamics of Stewart platform once we get the motion trajectory of platform. Because high external disturbance causes oscillations of each actuator, we designed a PID controller to decrease the effect of high external disturbance. We have known that I controller has good performance on decreasing oscillation in high frequency and steady state error. And D controller has performance on decreasing transient state error but it is poor at dealing with noise in high frequency. So, we have to choose a I controller with high gain and a D controller with low gain. The simulation results also showed that the oscillation can be almost ignored.

Herein only a simple dynamic model of vehicle has been used. In the future, a more complex model including the character of pedal or other factor such as air resistance or rough road can be considered. Combination with the technology of virtual reality, let people steeped in the powerful effect of sound and image. Moreover, the dynamic models of vehicle can be changed to other transportation suck as airplane, boat, or truck. In this way the simulation will be more realistic and simulation situation can be more diversified.

In this thesis, we designed a PID controller to control Stewart platform and got pretty good performance. However, the gain of PID controller may be not suitable one day because the oldness of mechanism. Furthermore the hydraulic system is a highly non-linear system. Many nonlinear control methods such as adaptive control, fuzzy control, or robust control can be applied on it.

REFERENCES

[1] D. Steward, “A platform with six degrees of freedom,” Proceedings of the Institution of Mechanical Engineers, vol. 180, pp. 371-386, 1965-1966.

[2] D. C. H Yang and T. W. Lee, ”Feasibility study of a platform type of robotic manipulators from a kinematic viewpoint,” Journal of Mechanisms, Transmissions, and Automation in Design, vol.106, no.1, pp.191-198,1984.

[3] E.F. Fichter, “A Stewart platform based manipulator：General theory and practical construction,” Int. Journal of Robotic Research, pp. 157-182, Summer 1986.

[4] W. Q. D. Do and D. C. H. Yang, “Inverse dynamic analysis and simulation of a platform type of robot,” Journal of Robotic Systems, vol. 5, no. 3, pp. 209-227, 1988.

[5] Liu, K., Fitzgerald, M., Dawson, D. W. and Lewis, F. L., “Modelling and control of a Stewart platform manipulator,” ASME DSC vol. 33, Control of Systems with Inexact Dynamic Models, pp. 83-89, 1991.

[6] Charles C. Nguyen, Zhen-Lei Zhou and Sami S. Antrazi, “Efficient computation of forward Kinematics and Jacobian matrix of a Stewart platform-based manipulator,” IEEE 1991.

[7] K. Liu, J. M. Fitzgerald, and F. L. Lewis, “Kinematic analysis of a Steward platform manipulator,” IEEE Trans. on Industrial Electronics, vol. 40, no. 2, pp. 282-293, 1993.

[8] Ji, Z., “Study of the effect of leg inertia in Stewart platforms,” Proceedings of the IEEE International conference of Robotics and Automation, vol. 1, pp. 121-126, 1993.

[9] B. Dasgupta and T. S. Mruthyunjaya, “A Newton-Euler formulation for the inverse dynamics of the Steward platform manipulator,” Mech. Mach. Theory, vol. 33, no. 8, pp. 1135-1152, 1998.

[10] Peter R. Grant and Lloyd D. Reid, “Motion washout filter tuning：Rules and requirements,” Journal of Aircraft, vol. 34, No. 2, March-April 1997.

[11] Nahon, M. A., and Reid, L. D., ”Simulator motion drive algorithms-A designer’s perspective,” Journal of Guidance, Control, and Dynamics, Vol. 13, No. 2, 1990, pp.356-362.

[12] G. R. Pitman, Inertial Guidance, John Wiley, New York, 1962.

[13] G. L. Zacharias, “Motion cue model for pilot-vehicle analysis,” AMRL-TR-8-2, 1978.

[14] L. D. Reid and M. A. Nahon, “Flight simulator motion-base drive algorithms:part 1-Developing and testing the equations,” UTLAS Report no. 296, CNISSN 0082-5255

[15] R. V. Dukkipati, M.O. M. Osman and S. S. Vallurupalli, “Adaptive active suspension to attain optimal performance and maintain static equilibrium level,” Int. J. of Vehicle Design, Vol. 14, pp. 471-496,1993.

[16]Krtolica and D. Hrovat, “Optimal active suspension control based on a half-car model,” Proceedings of the 29th Conference on Decision and Control, Honolulu, Hawaii , December 1990.

[17] Yi-Sheng Yao and Rama Chellappa, “Estimation of unstabilized components in vehicular motiom,” 1994.

[18] 謝國恩，沈勇全，陳雄章 譯，應用動力學，滄海書局

[19] J. S. Yun and H. S. Cho, “Adaptive model following control of electro-hydraulic velocity control systems subjected to unknown disturbances,” IEEE Proceedings, Vol. 135, No. 2, March 1988.

[20] 黃俊銘編譯，數值方法-使用 MATLAB 程式語言，全華科技圖書